

1 **Title:** Biaxial Testing System for Characterization of Mechanical and Rupture Properties of Small Samples

2 **Authors:** Andrea Corti <sup>a\*</sup>, Tariq Shameen <sup>a,1\*</sup>, Shivang Sharma <sup>a,2</sup>, Annalisa De Paolis PhD <sup>a</sup>, Luis Cardoso  
3 PhD <sup>a</sup>

4 \*Authors contributed equally

5 **Affiliations:** <sup>a</sup>City College of the City University of New York, New York, NY 10029, USA

6 **Present address:** <sup>1</sup>Memorial Sloan Kettering Cancer Center, New York, NY 10065, USA, <sup>2</sup>Rimsys  
7 Regulatory Management Software, Pittsburgh, PA 15212, USA

8 **Contact email:** [Cardoso@ccny.cuny.edu](mailto:Cardoso@ccny.cuny.edu)

### 9 **Authors Contribution Statement**

10 **Andrea Corti:** Conceptualization, Data Curation, Validation, Writing-review & editing; **Tariq Shameen:**  
11 Conceptualization, Data Curation, Validation, Writing-original draft; **Shivang Sharma:** Data Curation,  
12 Methodology; **Annalisa De Paolis:** Data Curation, Methodology; **Luis Cardoso:** Conceptualization,  
13 Supervision, Writing-review & editing, Funding acquisition.

### 14 **Abstract:**

15 The study of damage and rupture of soft tissues using a tensile testing system is essential to  
16 understand the limits of mechanical behavior and loss of function in diseased tissues. However,  
17 commercial material testing systems are often expensive and may not be fully suitable for rupture tests  
18 of small samples. While several research laboratories have developed custom, less expensive, uniaxial or  
19 biaxial devices, there is a need for an open source, inexpensive, accurate and easy to customize biaxial  
20 material testing system to perform rupture tests in small soft samples.

21 We designed a testing system (BiMaTS) that (a) was shown able to perform uniaxial and biaxial  
22 tests, (b) offers a large travel range for rupture tests of small samples, (c) maintains a centered field of  
23 view for effective strain mapping using digital image correlation, (d) provides a controlled temperature  
24 environment, (e) utilize many off-the-shelf components for easy manufacture and customization, and  
25 it is cost effective (~\$15K).

26 The instrument performance was characterized using 80%-scaled down, ASTM D412-C shaped  
27 PDMS samples. Our results demonstrate the ability of this open source, customizable, low-cost, biaxial  
28 materials testing system to successfully characterize the mechanical and rupture properties of small  
29 samples with high repeatability and accuracy.

30

### 31 **Keywords:**

32 Material Testing System, Uniaxial, Biaxial, Biomechanics, Tensile Testing, Rupture Testing.

33

34

35

36

37

1 **Table 1. Specifications table**

Hardware name	<i>Biaxial Material Testing System (BiMaTS)</i>
Subject area	● <i>Engineering and Material Science</i>
Hardware type	● <i>Other: Material Testing System</i>
Closest commercial analog	● <i>ADMET eXpert 8000 Series Planar Biaxial Test Machine</i> ● <i>ZwickRoell Biaxial Testing Machine</i> ● <i>TA Instruments: ElectroForce Planar Biaxial TestBench Instrument</i> ● <i>CellScale BioTester</i>
Open Source License	<i>CC-BY-4.0</i>
Cost of Hardware	<i>Approximate cost of hardware \$14,868.67</i>
Source File Repository	<a href="https://doi.org/10.17632/8sbwf397jk.1">https://doi.org/10.17632/8sbwf397jk.1</a>

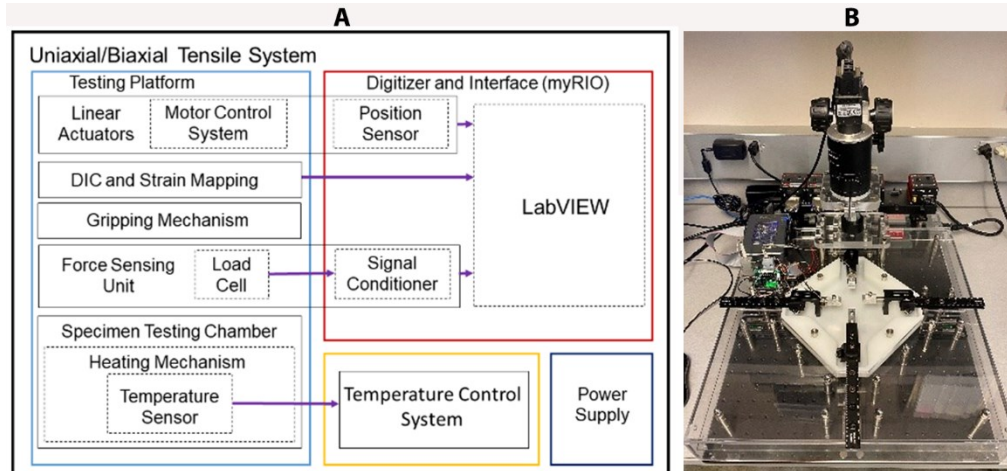
2 **1. Hardware in context**

3 The mechanical properties of soft tissues in the body change over time due to many biological,  
 4 environmental and extrinsic factors, including ageing, the onset of a pathology, or trauma. There exist  
 5 several approaches to characterize the biomechanical properties of tissues ex vivo, including tensile /  
 6 compression testing, indentation testing, ultrasound, atomic force microscopy, etc. In particular, the study  
 7 of damage and rupture of soft tissues using a uniaxial tensile testing system[1] is essential to understand  
 8 the limits of mechanical behavior and loss of function in diseased tissues[2]. However, commercial  
 9 material testing systems (e.g. Tytron 250 Microforce Testing System, ElectroForce Planar Biaxial  
 10 TestBench, Cell Scale BioTester[3, 4], etc.) are often expensive (\$50K-\$100K+) and several research  
 11 laboratories have developed custom, less expensive, uniaxial or biaxial devices [5-12], or open source [13].  
 12 Also, most systems may not be suitable for rupture tests of small samples due to a limited travel range,  
 13 their gripping mechanism [14], and/or load cell range. Thus, there is a need for an open source biaxial  
 14 material testing system to perform rupture tests in soft tissues, inexpensive, accurate and easy to  
 15 customize by the researcher.

16 In this study, we report the design of an open source, low-cost biomechanical testing system that  
 17 allows us to characterize the mechanical and rupture properties of small samples with high accuracy and  
 18 precision. The proposed biaxial materials testing system (BiMaTS) comprises four high performance  
 19 actuators with inline load cells (8.90 N), high resolution imaging with image-based strain measurement  
 20 tools[15, 16], integrated temperature controlled media bath, and a LabView-based user interface for  
 21 automated computer controlled testing with real-time feedback. The BiMaTS is able (1) to perform  
 22 uniaxial and biaxial tests, (2) offers a large travel range (100mm) for rupture tests of small samples (~5-  
 23 25mm long), (3) maintains a centered field of view for effective strain mapping using digital image  
 24 correlation (DIC), (4) provides a controlled environment for testing of biological tissues under immersion  
 25 (e.g. phosphate saline solution) and physiological temperature control, and (5) utilize many off-the-shelf  
 26 components for easy manufacture. The repeatability, accuracy and overall performance of the instrument  
 27 (i.e. displacement, actuator velocity, force, temperature, gripping slippage, strain mapping) was  
 28 characterized using Polydimethylsiloxane (PDMS) samples with ASTM D412-C standard shape, following  
 29 the recommended testing guidelines for rubber-like materials.

1           **2. Hardware description.**

2           The BiMaTS (**Figure 1**) comprises six building blocks or subsystems: (1) testing platform; (2)  
3 specimen testing chamber; (3) force sensing unit; (4) sample gripping mechanism; (5) optical strain  
4 mapping; and (6) computer and Graphical User Interface (GUI) for control and operation of the system.

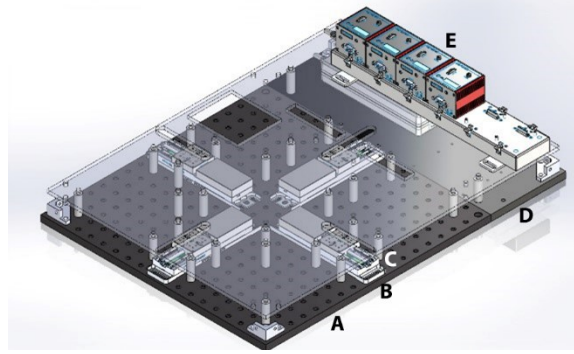


5  
6 **Figure 1. (A)** Biaxial Material Testing System (BiMaTS) building blocks: testing platform; specimen testing  
7 chamber; force sensing unit; tissue gripping mechanism; optical strain mapping; and graphical user  
8 interface for control and operation of the system. **(B)** Photograph of the BiMaTS instrument.

9

10           **2.1 Testing Platform**

11           The testing platform consists of a rigid aluminum breadboard typically used for laser and optical  
12 applications (**Figure 2**). This breadboard provides an excellent means to adjust the location of any  
13 components while maintaining excellent alignment among actuators. Four linear actuators (Thorlabs  
14 MTS50-Z8-50mm motorized translation stage) were positioned in a cruciform configuration to allow the  
15 stretching of samples along two orthogonal axes, while maintaining the sample's region of interest at the  
16 center of the field of view. Each linear actuator has a 50 mm range of motion with a 25 lb horizontal load  
17 capacity, 2.4 mm/s maximal velocity, and 4.5 mm/s<sup>2</sup> maximal acceleration (full technical specifications are  
18 found at [https://www.thorlabs.com/newgrouppage9.cfm?objectgroup\\_id=3002&pn=MTS50-Z8](https://www.thorlabs.com/newgrouppage9.cfm?objectgroup_id=3002&pn=MTS50-Z8)).  
19 Therefore, two combined actuators lead to a full 100mm range of motion in X and Y directions. DC Servo  
20 motor actuators are powered and controlled by a DC Servo Motor Driver (Thorlabs' K-Cube Series  
21 KBD101s), which provide closed-loop feedback control via built-in Hall Effect position encoders for precise  
22 motion of the actuator (minimum achievable incremental movement of 0.05µm, minimum repeatable  
23 incremental movement of 0.8µm, bidirectional repeatability of 1.6µm, backlash <6µm, and home  
24 location accuracy of ±4.0 µm).

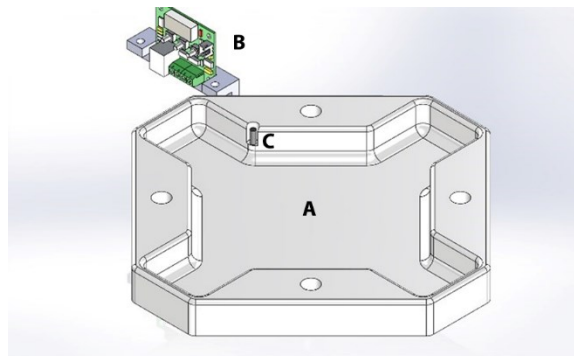


1  
 2 **Figure 2.** BiMaTS testing platform. (A) breadboard, (B) Breadboard Mounting Adapter (MTS50A-Z8), (C)  
 3 linear actuator (MTS50-Z8), (D) back extension plate, (E) DC Servo Motor Driver (KBD101).

4

5 **2.2 Specimen Testing Chamber**

6 The specimen testing chamber has a cross-shaped design made of biocompatible  
 7 Polytetrafluoroethylene (PTFE) and was designed for examination of samples in air and under fluid  
 8 immersion (**Figure 3**). To control the fluid temperature used for testing samples under immersion, the  
 9 chamber has a Peltier ceramic actuator driven by a W1209 temperature control board. The Peltier plate  
 10 and W1209 control board are powered up by independent power supplies. The heating side of the Peltier  
 11 thermal actuator was attached to a 10 mm x 10 mm x 1 mm stainless steel plate that lies beneath the  
 12 chamber's base. The W1209 reads the fluid temperature using a 4mm diameter sensor that was placed  
 13 within the chamber and determines whether the Peltier plate should be powered up or down to maintain  
 14 the chamber fluid within  $37 \pm 1^\circ\text{C}$ . The operation settings of the W1209 temperature control circuit  
 15 include the P0 parameter, which was set to 'H' as the chamber needs to be heated. The target  
 16 temperature was set to  $37.0^\circ\text{C}$ , with the hysteresis parameter P1 selected at  $0.1^\circ\text{C}$ . The lower limit,  
 17 parameter P3, of the temperature range was configured to  $35.0^\circ\text{C}$ , and the upper limit/relay off,  
 18 parameter P2 and P6 were chosen to reach  $40.0^\circ\text{C}$ . The temperature reading of the circuit was calibrated  
 19 and adjusted using parameter P4 to match the readings of a reference digital thermometer.



20

21 **Figure 3.** Specimen testing chamber. (A) specimen testing chamber has a cross-shaped design  
 22 made of biocompatible Polytetrafluoroethylene (PTFE), (B) Temperature control board (W1209), (C)  
 23 temperature sensor.

### 2.3 Force Sensing unit

Each linear actuator has an adapter plate (MTSA1) and two stainless steel posts that connect the device to an actuation arm (**Figure 4**). The actuation arm comprises a 6 inches dovetail optical rail (RLA0600), a rail carrier (RC1) and a right angle bracket (AB90C). The carrier can be placed onto the rail anywhere along its length without requiring access to the rail ends. The spring-loaded plunger built into the locking thumbscrew provides wobble-free translation as the carrier slides along the rail. A low-friction joint between the right angle bracket and the rail carrier was implemented using two ball bearings and a stainless steel dowel pin, so that the angle bracket can rotate freely. A tread adapter (MSA25) was then used to secure the fixed end of a sub-miniature load cell (Honeywell, model 31, 2000g) to one of the ¼"-20 threaded holes in the bracket. The movable end of the load cell was directly connected to the sample clamp. The cable from the load cell was linked to a load cell signal conditioner and digitizing circuit (HX711 Sensor) using a DB-09 connector, so that the load cell can be easily replaced if needed. The HX711 board has a full Wheatstone bridge configuration to sense changes in the load cell, followed by the HX711 microchip, a precision 24-bit analog to digital converter with low-noise programmable gain amplifier. The HX711 uses a two-wire interface (Clock and Data) for synchronization and data transfer (80SPS) with a GPIO. Here we use a portable reconfigurable I/O device (myRIO-1900, National instruments) for real time acquisition of load cell data from the HX711 board, and for transferring the data from the myRIO-1900 into a computer for recording and visualization of data using a graphical user interface in LabView.

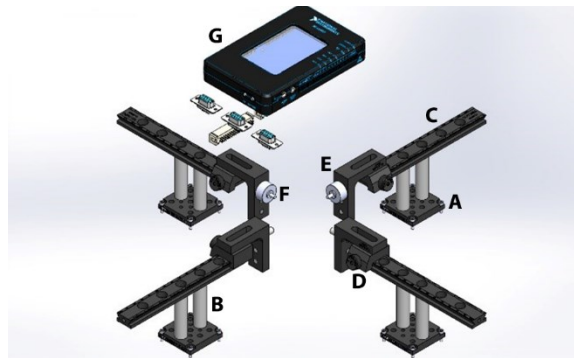
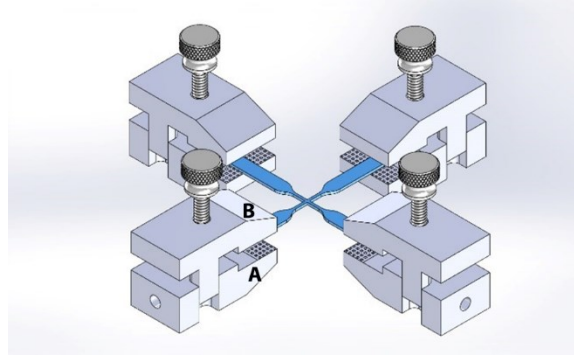


**Figure 4.** Force sensing unit. (A) Linear actuator adapter plate (MTSA1), (B) stainless steel posts, (C) actuation arm - dovetail optical rail (RLA0600), (D) rail carrier (RC1), (E) right angle bracket (AB90C), (F) sub-miniature load cell (Honeywell, model 31, 2000g), (G) portable reconfigurable I/O device (myRIO-1900, National instruments).

### 2.4 Sample Gripping mechanism

The gripping mechanism consists of four small custom made clamps (**Figure 5**). Each clamp comprises a bottom jaw, a top closing jaw, and one thumbscrew. The bottom piece is firmly attached to the mobile end of the load cell or the right angle bracket. The top jaw of the clamp can be moved up and down, but remains well aligned to the bottom piece due to a vertical slot and pin built in within the clamp design. The thumbscrew secures the two jaws of the clamp, while maintaining their surfaces well aligned and parallel to provide a uniform holding force on the sample. The top portion of the clamp is removed

1 prior to carefully placing and aligning the sample on top of the bottom jaw. Then, the top jaw is placed  
2 and secured via the clamp screw. We manufactured clamps made of acrylic, aluminum and 3D printed  
3 using ABS. While all these materials were effective when testing soft materials and tissues, the aluminum  
4 clamps are in general considered more durable than the other tested materials.



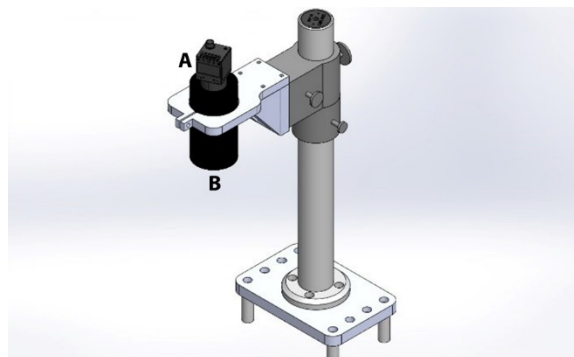
5

6 **Figure 5.** Sample gripping mechanism. (A) aluminum tissue clamp bottom jaw, (B) top jaw, (C)  
7 biaxial sample.

8

### 9 2.5 Digital Image Correlation System

10 Throughout a uniaxial or biaxial test, images are taken within a Region of Interest (ROI) of the  
11 sample, and both deformation and strains are calculated within the ROI using Digital Image Correlation  
12 (DIC). This subsystem comprises a high-resolution camera (FLIR Blackfly S, BFS-U3-200S6C-C, 20Mp, 18FPS,  
13 CMOS Sony IMX183 sensor) and a Machine Vision Lens (Tamron M111FM25), which are positioned  
14 directly above the testing chamber using a custom camera holder (**Figure 6**). The camera is connected to  
15 the LabVIEW program via a USB3 Vision V1.0 connection port. Within the program, the NI-IMAQ module  
16 is utilized to acquire images for the entire duration of the test. Once the test is completed, the images are  
17 loaded into the image analyzer program, GOM Correlate (<https://www.gom.com/en/>). This program is  
18 used to calculate and display the strain map experienced by the specimen throughout the duration of the  
19 experiment.



20

21 **Figure 6.** Digital image correlation. (A) high-resolution camera (FLIR Blackfly S, BFS-U3-200S6C-C)  
22 and (B) Machine Vision Lens (Tamron M111FM25).

23

## 2.6 Graphical User Interface.

A graphical user interface (GUI) was developed in LabView to control the operation of the system (Figure 7). The GUI is split into three main sections, the hardware driver section on the left of the GUI presents the software interface used for communication with the DC servo controller hardware and to set up the working velocity and acceleration of actuators. The middle section of the GUI comprises a Tab control that contains three tabs for either performing preconditioning, uniaxial or biaxial tests. Finally, the right hand side of the GUI has the control boxes where the user can input the desired X and/or Y displacement(s) range, a graph to visualize the measured X and/or Y force(s), and a control to tare the force reading(s) prior to initiate a test. The GUI also has user controls for defining the name and folder where images will be recorded, and a window with real time image of the field of view prior to initiate a test. Data is recorded using the TDMS format (Labview, National Instruments), and images are stored as JPEG. Force, displacement, and time can be easily exported into Matlab for analysis of engineering stresses and strains. The sequence of images taken during the test are also exported into GOM Correlate Software to calculate the true stress and strain in the center region of interest in the sample.

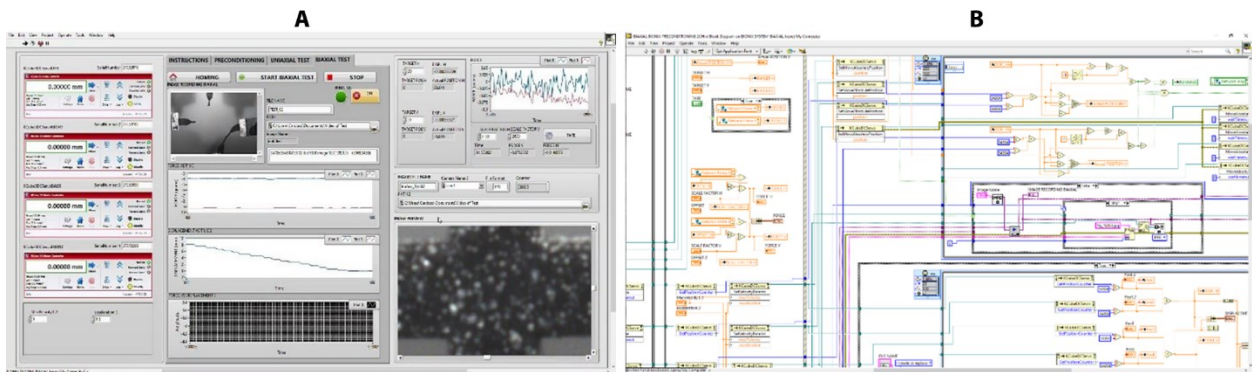


Figure 7. Graphical user interface. (A) LabView front panel used for operation of the system and visualization of data, and (B) LabView block diagram of the operational system.

## 2.7 Key aspects of the system

Overall, the BiMaTS is a low cost device with high precision and accuracy of motion, that offers a large range of displacement necessary for the mechanical testing of samples up to rupture in dry or under immersion conditions with temperature control. The system can perform uniaxial and biaxial tensile testing, is fully automated and customizable by the researcher. The BiMaTS has the capability of characterizing the tensile properties of soft materials in the following manner:

- The system has large displacement range to test samples under uniaxial or biaxial configuration up to rupture
- The small load cell rating allows accurate measurement of reaction forces in soft samples, and it is fully customizable to higher load ranges
- High-resolution images and DIC method are used for non-invasive assessment of the specimen's strain map

- Fully automated system with configurable parameters (e.g. range of motion, velocity, acceleration, preconditioning cycles, images field of view, etc.)
- The clamps have small weight, are self-aligning, minimize slippage as well as sample rupture at the interface with the grip
- Integrated temperature control system for immersion testing while maintaining physiological conditions
- Cost is under **\$15,000** which is significantly lower than commercial biaxial testing systems

### 3. Design files

#### Design Files Summary

**Table 2.** Design files name, type, open source license and repository location.

Design file name	File type	Open source license	Location of the file
<b>Testing platform</b>			
Breadboard	CAD	CC-BY-4.0	<a href="https://doi.org/10.17632/8sbwf397jk.1">https://doi.org/10.17632/8sbwf397jk.1</a>
Back-end Plate	CAD	CC-BY-4.0	<a href="https://doi.org/10.17632/8sbwf397jk.1">https://doi.org/10.17632/8sbwf397jk.1</a>
Base Plate for Stage	CAD	CC-BY-4.0	<a href="https://doi.org/10.17632/8sbwf397jk.1">https://doi.org/10.17632/8sbwf397jk.1</a>
Motorized Translation Stage	CAD	CC-BY-4.0	<a href="https://doi.org/10.17632/8sbwf397jk.1">https://doi.org/10.17632/8sbwf397jk.1</a>
USB Controller Hub and Power Supply for Six K-Cubes	CAD	CC-BY-4.0	<a href="https://doi.org/10.17632/8sbwf397jk.1">https://doi.org/10.17632/8sbwf397jk.1</a>
K-Cube Brushed DC Servo Motor Controller	CAD	CC-BY-4.0	<a href="https://doi.org/10.17632/8sbwf397jk.1">https://doi.org/10.17632/8sbwf397jk.1</a>
Round standoff 0.5 in	CAD	CC-BY-4.0	<a href="https://doi.org/10.17632/8sbwf397jk.1">https://doi.org/10.17632/8sbwf397jk.1</a>
Round standoff 1.25 in (0.75 + 0.5 in)	CAD	CC-BY-4.0	<a href="https://doi.org/10.17632/8sbwf397jk.1">https://doi.org/10.17632/8sbwf397jk.1</a>
Round standoff 1.5 in	CAD	CC-BY-4.0	<a href="https://doi.org/10.17632/8sbwf397jk.1">https://doi.org/10.17632/8sbwf397jk.1</a>
Round standoff 2.0 in	CAD	CC-BY-4.0	<a href="https://doi.org/10.17632/8sbwf397jk.1">https://doi.org/10.17632/8sbwf397jk.1</a>
Front Panel	CAD	CC-BY-4.0	<a href="https://doi.org/10.17632/8sbwf397jk.1">https://doi.org/10.17632/8sbwf397jk.1</a>
Left Panel	CAD	CC-BY-4.0	<a href="https://doi.org/10.17632/8sbwf397jk.1">https://doi.org/10.17632/8sbwf397jk.1</a>
Right Panel	CAD	CC-BY-4.0	<a href="https://doi.org/10.17632/8sbwf397jk.1">https://doi.org/10.17632/8sbwf397jk.1</a>
Back Panel	CAD	CC-BY-4.0	<a href="https://doi.org/10.17632/8sbwf397jk.1">https://doi.org/10.17632/8sbwf397jk.1</a>
Back Panel Top	CAD	CC-BY-4.0	<a href="https://doi.org/10.17632/8sbwf397jk.1">https://doi.org/10.17632/8sbwf397jk.1</a>
Case cover middle	CAD	CC-BY-4.0	<a href="https://doi.org/10.17632/8sbwf397jk.1">https://doi.org/10.17632/8sbwf397jk.1</a>
Case cover Top	CAD	CC-BY-4.0	<a href="https://doi.org/10.17632/8sbwf397jk.1">https://doi.org/10.17632/8sbwf397jk.1</a>
Corner adapter	CAD	CC-BY-4.0	<a href="https://doi.org/10.17632/8sbwf397jk.1">https://doi.org/10.17632/8sbwf397jk.1</a>
Cap Nuts	CAD	CC-BY-4.0	<a href="https://doi.org/10.17632/8sbwf397jk.1">https://doi.org/10.17632/8sbwf397jk.1</a>
Power Module	CAD	CC-BY-4.0	<a href="https://doi.org/10.17632/8sbwf397jk.1">https://doi.org/10.17632/8sbwf397jk.1</a>
Flanged Screw-to-Expand Inserts for Plastic	CAD	CC-BY-4.0	<a href="https://doi.org/10.17632/8sbwf397jk.1">https://doi.org/10.17632/8sbwf397jk.1</a>
Flanged Button Head Screws	CAD	CC-BY-4.0	<a href="https://doi.org/10.17632/8sbwf397jk.1">https://doi.org/10.17632/8sbwf397jk.1</a>
<b>Specimen Testing Chamber</b>			
Testing chamber	CAD	CC-BY-4.0	<a href="https://doi.org/10.17632/8sbwf397jk.1">https://doi.org/10.17632/8sbwf397jk.1</a>
Pedestal Pillar Post 1.5in	CAD	CC-BY-4.0	<a href="https://doi.org/10.17632/8sbwf397jk.1">https://doi.org/10.17632/8sbwf397jk.1</a>
Stainless steel plate	CAD	CC-BY-4.0	<a href="https://doi.org/10.17632/8sbwf397jk.1">https://doi.org/10.17632/8sbwf397jk.1</a>
Peltier plate	CAD	CC-BY-4.0	<a href="https://doi.org/10.17632/8sbwf397jk.1">https://doi.org/10.17632/8sbwf397jk.1</a>
Thermostat	CAD	CC-BY-4.0	<a href="https://doi.org/10.17632/8sbwf397jk.1">https://doi.org/10.17632/8sbwf397jk.1</a>
Thermostat Bracket	CAD	CC-BY-4.0	<a href="https://doi.org/10.17632/8sbwf397jk.1">https://doi.org/10.17632/8sbwf397jk.1</a>
Temperature sensor	CAD	CC-BY-4.0	<a href="https://doi.org/10.17632/8sbwf397jk.1">https://doi.org/10.17632/8sbwf397jk.1</a>
tmp60 power supply	CAD	CC-BY-4.0	<a href="https://doi.org/10.17632/8sbwf397jk.1">https://doi.org/10.17632/8sbwf397jk.1</a>
tmp30 power supply	CAD	CC-BY-4.0	<a href="https://doi.org/10.17632/8sbwf397jk.1">https://doi.org/10.17632/8sbwf397jk.1</a>
<b>Force sensing unit</b>			
Adapter Plate for MTS50 Stages	CAD	CC-BY-4.0	<a href="https://doi.org/10.17632/8sbwf397jk.1">https://doi.org/10.17632/8sbwf397jk.1</a>
Dovetail Optical Rail	CAD	CC-BY-4.0	<a href="https://doi.org/10.17632/8sbwf397jk.1">https://doi.org/10.17632/8sbwf397jk.1</a>
Dovetail Rail Carrier	CAD	CC-BY-4.0	<a href="https://doi.org/10.17632/8sbwf397jk.1">https://doi.org/10.17632/8sbwf397jk.1</a>
Right-Angle Bracket	CAD	CC-BY-4.0	<a href="https://doi.org/10.17632/8sbwf397jk.1">https://doi.org/10.17632/8sbwf397jk.1</a>
Thread Adapter	CAD	CC-BY-4.0	<a href="https://doi.org/10.17632/8sbwf397jk.1">https://doi.org/10.17632/8sbwf397jk.1</a>

Honeywell load sensor	CAD	CC-BY-4.0	<a href="https://doi.org/10.17632/8sbwf397jk.1">https://doi.org/10.17632/8sbwf397jk.1</a>
National Instruments -myRIO-1900	CAD	CC-BY-4.0	<a href="https://doi.org/10.17632/8sbwf397jk.1">https://doi.org/10.17632/8sbwf397jk.1</a>
HX711 Weighing Sensor	CAD	CC-BY-4.0	<a href="https://doi.org/10.17632/8sbwf397jk.1">https://doi.org/10.17632/8sbwf397jk.1</a>
DB-9F-2	CAD	CC-BY-4.0	<a href="https://doi.org/10.17632/8sbwf397jk.1">https://doi.org/10.17632/8sbwf397jk.1</a>
CONN HEADER 34POS IDC	CAD	CC-BY-4.0	<a href="https://doi.org/10.17632/8sbwf397jk.1">https://doi.org/10.17632/8sbwf397jk.1</a>
<b>Sample gripping mechanism</b>			
Metal Grip Top	CAD	CC-BY-4.0	<a href="https://doi.org/10.17632/8sbwf397jk.1">https://doi.org/10.17632/8sbwf397jk.1</a>
Metal Grip Bottom	CAD	CC-BY-4.0	<a href="https://doi.org/10.17632/8sbwf397jk.1">https://doi.org/10.17632/8sbwf397jk.1</a>
Thumbscrew	CAD	CC-BY-4.0	<a href="https://doi.org/10.17632/8sbwf397jk.1">https://doi.org/10.17632/8sbwf397jk.1</a>
Type-D biaxial sample	CAD	CC-BY-4.0	<a href="https://doi.org/10.17632/8sbwf397jk.1">https://doi.org/10.17632/8sbwf397jk.1</a>
Sample_Holder_Base	CAD	CC-BY-4.0	<a href="https://doi.org/10.17632/8sbwf397jk.1">https://doi.org/10.17632/8sbwf397jk.1</a>
Sample_Holder_Top	CAD	CC-BY-4.0	<a href="https://doi.org/10.17632/8sbwf397jk.1">https://doi.org/10.17632/8sbwf397jk.1</a>
<b>Optical Strain mapping</b>			
Camera Base Plate	CAD	CC-BY-4.0	<a href="https://doi.org/10.17632/8sbwf397jk.1">https://doi.org/10.17632/8sbwf397jk.1</a>
Dynamically Damped Post	CAD	CC-BY-4.0	<a href="https://doi.org/10.17632/8sbwf397jk.1">https://doi.org/10.17632/8sbwf397jk.1</a>
Lens Holder Assembly	CAD	CC-BY-4.0	<a href="https://doi.org/10.17632/8sbwf397jk.1">https://doi.org/10.17632/8sbwf397jk.1</a>
Camera	CAD	CC-BY-4.0	<a href="https://doi.org/10.17632/8sbwf397jk.1">https://doi.org/10.17632/8sbwf397jk.1</a>
Lens	CAD	CC-BY-4.0	<a href="https://doi.org/10.17632/8sbwf397jk.1">https://doi.org/10.17632/8sbwf397jk.1</a>

1  
2  
3  
4

#### 4. Bill of Materials

**Table 3.** Bill of materials, designator, component, unit cost, total cost, source and type of material.

Designator	Component	Number	Cost per unit -currency	Total cost - currency	Source of materials	Material type
<b>Testing Platform</b>						
Breadboard	MB18 18" x 18" x 1/2", 1/4"-20 Taps, thorlabs	1	\$281.56	\$281.56	<a href="https://www.thorlabs.com/thorproduct.cfm?partnumber=MB18">https://www.thorlabs.com/thorproduct.cfm?partnumber=MB18</a>	Metal
Back-end Plate	8560K266	1	\$59.08	\$59.08	<a href="https://www.mcmaster.com/catalog/127/3896">https://www.mcmaster.com/catalog/127/3896</a>	Acrylic
Base Plate for Stage	MTS50A-Z8	4	\$86.03	\$344.12	<a href="https://www.thorlabs.com/newgrouppage9.cfm?objectgroup_id=3002&amp;pn=MTS50A-Z8#3116">https://www.thorlabs.com/newgrouppage9.cfm?objectgroup_id=3002&amp;pn=MTS50A-Z8#3116</a>	Metal
Motorized Translation Stage	MTS50-Z8 50 mm (1.97"), 8-32 and 4-40 Taps	4	\$1,151.38	\$4,605.52	<a href="https://www.thorlabs.com/newgrouppage9.cfm?objectgroup_id=3002&amp;pn=MTS50-Z8#3006">https://www.thorlabs.com/newgrouppage9.cfm?objectgroup_id=3002&amp;pn=MTS50-Z8#3006</a>	Metal
USB Controller Hub and Power Supply for Six K-Cubes	KCH601	1	\$635.20	\$635.20	<a href="https://www.thorlabs.com/newgrouppage9.cfm?objectgroup_id=2424&amp;pn=KCH601#13030">https://www.thorlabs.com/newgrouppage9.cfm?objectgroup_id=2424&amp;pn=KCH601#13030</a>	Electronic Comp
K-Cube Brushed DC Servo Motor Controller	KDC101	4	\$677.41	\$2,709.64	<a href="https://www.thorlabs.com/newgrouppage9.cfm?objectgroup_id=2419&amp;pn=KDC101#5077">https://www.thorlabs.com/newgrouppage9.cfm?objectgroup_id=2419&amp;pn=KDC101#5077</a>	Electronic Comp
Standoff 0.5 in	91125A382	28	\$3.20	\$89.60	<a href="https://www.mcmaster.com/catalog/127/3539/">https://www.mcmaster.com/catalog/127/3539/</a>	Metal
Standoff 0.75 in	91125A392	24	\$3.41	\$81.84	<a href="https://www.mcmaster.com/catalog/127/3539/">https://www.mcmaster.com/catalog/127/3539/</a>	Metal
Standoff 1.5 in	91125A422	31	\$3.92	\$121.52	<a href="https://www.mcmaster.com/catalog/127/3539/">https://www.mcmaster.com/catalog/127/3539/</a>	Metal
Standoff 2.0 in	91125A652	12	\$3.95	\$47.40	<a href="https://www.mcmaster.com/catalog/127/3539/">https://www.mcmaster.com/catalog/127/3539/</a>	
Front Panel	1227T259	2ft	\$3.48	\$6.96	<a href="https://www.mcmaster.com/catalog/127/3897/">https://www.mcmaster.com/catalog/127/3897/</a>	Acrylic
Left Panel	1227T259	2ft	\$3.48	\$6.96	<a href="https://www.mcmaster.com/catalog/127/3897/">https://www.mcmaster.com/catalog/127/3897/</a>	Acrylic
Right Panel	1227T259	2ft	\$3.48	\$6.96	<a href="https://www.mcmaster.com/catalog/127/3897/">https://www.mcmaster.com/catalog/127/3897/</a>	Acrylic
Back Panel	1227T259	2ft	\$3.48	\$6.96	<a href="https://www.mcmaster.com/catalog/127/3897/">https://www.mcmaster.com/catalog/127/3897/</a>	Acrylic
Back Panel Top	1227T259	2ft	\$3.48	\$6.96	<a href="https://www.mcmaster.com/catalog/127/3897/">https://www.mcmaster.com/catalog/127/3897/</a>	Acrylic

Case cover middle	8589K83	1	\$35.42	\$35.42	<a href="https://www.mcmaster.com/catalog/127/3899/">https://www.mcmaster.com/catalog/127/3899/</a>	Acrylic
Case cover Top	8589K83	1	\$35.42	\$35.42	<a href="https://www.mcmaster.com/catalog/127/3899/">https://www.mcmaster.com/catalog/127/3899/</a>	Acrylic
Corner adapter	1227T529	2ft	\$6.67	\$13.34	<a href="https://www.mcmaster.com/catalog/127/3897/">https://www.mcmaster.com/catalog/127/3897/</a>	Acrylic
Cap Nuts	91855A520	2 pk	\$8.17	\$16.34	<a href="https://www.mcmaster.com/catalog/127/3460/">https://www.mcmaster.com/catalog/127/3460/</a>	Metal
Power Module	DD11.0111.111	1	\$11.86	\$11.86	<a href="https://www.newark.com/schurter/dd11-0111-1111/c14-inlet-250vac-10a-quick-connect/dp/48M7010">https://www.newark.com/schurter/dd11-0111-1111/c14-inlet-250vac-10a-quick-connect/dp/48M7010</a>	Electric comp
Flanged Screw-to-Expand Inserts for Plastic	95110A113	2 pk	\$11.67	\$23.34	<a href="https://www.mcmaster.com/catalog/127/3568/">https://www.mcmaster.com/catalog/127/3568/</a>	Metal
Flanged Button Head Screws	96660A156	2 pk	\$11.69	\$23.38	<a href="https://www.mcmaster.com/catalog/127/3268/">https://www.mcmaster.com/catalog/127/3268/</a>	Metal
<b>Sample testing chamber</b>						
Testing Chamber	8619K491	1	\$30.77	\$30.77	<a href="https://www.mcmaster.com/catalog/127/3924/">https://www.mcmaster.com/catalog/127/3924/</a>	Polyethylene HDPE
Pedestal Pillar Post 1.5in	TRP1.5	4	\$21.64	\$86.56	<a href="https://www.thorlabs.com/newgrouppage9.cfm?objectgroup_id=10491&amp;pn=TRP1.5#10495">https://www.thorlabs.com/newgrouppage9.cfm?objectgroup_id=10491&amp;pn=TRP1.5#10495</a>	Metal
Stainless Steel plate, 0.024" thick 6"x6"	8983K111	1	\$3.87	\$3.87	<a href="https://www.mcmaster.com/8983K111/">https://www.mcmaster.com/8983K111/</a>	Metal
Peltier plate	TEC1-12706	1	\$9.99	\$9.99	<a href="https://www.amazon.com/DAOKI-TEC1-12706-Heatsink-Thermoelectric-Cooling/dp/B00XT0OZY0/ref=sr_1_23?dchild=1&amp;keywords=peltier+plate&amp;qid=1631740703&amp;s=industrial&amp;sr=1-23">https://www.amazon.com/DAOKI-TEC1-12706-Heatsink-Thermoelectric-Cooling/dp/B00XT0OZY0/ref=sr_1_23?dchild=1&amp;keywords=peltier+plate&amp;qid=1631740703&amp;s=industrial&amp;sr=1-23</a>	component
Thermostat and temperature sensor	W1209	1	\$7.89	\$7.89	<a href="https://www.amazon.com/Temperature-Controller-Thermostat-Envistia-Mall/dp/B07N3Y2M3Z/ref=sr_1_14?dchild=1&amp;keywords=W1209&amp;qid=1631740609&amp;s=industrial&amp;sr=1-14">https://www.amazon.com/Temperature-Controller-Thermostat-Envistia-Mall/dp/B07N3Y2M3Z/ref=sr_1_14?dchild=1&amp;keywords=W1209&amp;qid=1631740609&amp;s=industrial&amp;sr=1-14</a>	Electronic component
Thermostat Bracket	9115K43	1	\$36.39	\$36.39	<a href="https://www.mcmaster.com/acrylic/thickness~1-2/width~1/length~12/">https://www.mcmaster.com/acrylic/thickness~1-2/width~1/length~12/</a>	Acrylic
tmp60 power supply	TMP 60112	1	\$71.90	\$71.90	<a href="https://www.digikey.com/en/products/detail/traco-power/TMP-60112/9343878">https://www.digikey.com/en/products/detail/traco-power/TMP-60112/9343878</a>	Electric comp
tmp30 power supply	TMP 30112	1	\$55.30	\$55.30	<a href="https://www.digikey.com/en/products/detail/traco-power/TMP-30112/9343860">https://www.digikey.com/en/products/detail/traco-power/TMP-30112/9343860</a>	Electric comp
<b>Force sensing unit</b>						
Adapter Plate for Stage	MTSA1	4	\$47.35	\$189.40	<a href="https://www.thorlabs.com/newgrouppage9.cfm?objectgroup_id=3423&amp;pn=MTSA1#7391">https://www.thorlabs.com/newgrouppage9.cfm?objectgroup_id=3423&amp;pn=MTSA1#7391</a>	Metal
Dovetail Optical Rail	RLA0600	4	\$45.72	\$182.88	<a href="https://www.thorlabs.com/newgrouppage9.cfm?objectgroup_id=30&amp;pn=RLA0600#8294">https://www.thorlabs.com/newgrouppage9.cfm?objectgroup_id=30&amp;pn=RLA0600#8294</a>	Metal
Dovetail Rail Carrier	RC1	4	\$26.94	\$107.76	<a href="https://www.thorlabs.com/newgrouppage9.cfm?objectgroup_id=8295&amp;pn=RC1#8296">https://www.thorlabs.com/newgrouppage9.cfm?objectgroup_id=8295&amp;pn=RC1#8296</a>	Metal
Slim Right-Angle Bracket	AB90C	4	\$27.85	\$111.40	<a href="https://www.thorlabs.com/newgrouppage9.cfm?objectgroup_id=223&amp;pn=AB90C#2119">https://www.thorlabs.com/newgrouppage9.cfm?objectgroup_id=223&amp;pn=AB90C#2119</a>	Metal
National Instruments - myRIO-1900	782692-01	1	\$571.50	\$571.50	<a href="https://www.ni.com/en-us/shop/hardware/products/myrio-student-embedded-device.html?modelId=125751">https://www.ni.com/en-us/shop/hardware/products/myrio-student-embedded-device.html?modelId=125751</a>	Electronic component
Honeywell load sensor	060-1432-07	2	\$1,288.77	\$2,577.54	<a href="https://www.digikey.com/en/products/detail/honeywell-sensing-and-productivity-solutions-t-m/060-1432-07/5055799">https://www.digikey.com/en/products/detail/honeywell-sensing-and-productivity-solutions-t-m/060-1432-07/5055799</a>	Sensor
Thread Adapter	AE6E25E	4	\$4.53	\$18.12	<a href="https://www.thorlabs.com/newgrouppage9.cfm?objectgroup_id=1745&amp;pn=AE6E25E#1439">https://www.thorlabs.com/newgrouppage9.cfm?objectgroup_id=1745&amp;pn=AE6E25E#1439</a>	Metal
HX711 Weighing Sensor	HX711	3	\$5.69 / 3 pc	\$5.69	<a href="https://www.amazon.com/HiLetgo-Weighing-Dual-Channel-Precision-Pressure/dp/B00XRRNCOO/ref=pd_lpo_2?pd_rd_i=B00XRRNCOO&amp;psc=1">https://www.amazon.com/HiLetgo-Weighing-Dual-Channel-Precision-Pressure/dp/B00XRRNCOO/ref=pd_lpo_2?pd_rd_i=B00XRRNCOO&amp;psc=1</a>	Electronic component

DB-9F-2	2301838-1	3	\$2.21	\$6.63	<a href="https://www.digikey.com/en/products/detail/te-connectivity-amp-connectors/2301838-1/7776535">https://www.digikey.com/en/products/detail/te-connectivity-amp-connectors/2301838-1/7776535</a>	Connector
CONN HEADER 34POS IDC	732-5457-ND	2	\$5.86	\$11.72	<a href="https://www.digikey.com/en/products/detail/w%C3%BCrth-elektronik/61203425821/4846942">https://www.digikey.com/en/products/detail/w%C3%BCrth-elektronik/61203425821/4846942</a>	Connector
34 Position Cable Assembly 0.500'	H3CCH-3406G	2	\$1.57	\$3.14	<a href="https://www.digikey.com/en/products/detail/assmann-aws-components/H3CCH-3406G/1218569">https://www.digikey.com/en/products/detail/assmann-aws-components/H3CCH-3406G/1218569</a>	Cable assembly
<b>Sample gripping mech.</b>						
Metal Grip Top	8975K618	1	\$4.49	\$4.49	<a href="https://www.mcmaster.com/catalog/127/3979/">https://www.mcmaster.com/catalog/127/3979/</a>	Metal
Metal Grip Bottom	8975K618	1	\$4.49	\$4.49	<a href="https://www.mcmaster.com/catalog/127/3979/">https://www.mcmaster.com/catalog/127/3979/</a>	Metal
Type-D biaxial sample	Sylgard 184	1/10	\$15.30	\$15.30	<a href="https://www.amazon.com/Electron-Microscopy-Sciences-Sylgard-184/dp/B00K335I0G">https://www.amazon.com/Electron-Microscopy-Sciences-Sylgard-184/dp/B00K335I0G</a>	PDMS
Sample Holder Base	1227T459	1	\$6.07	\$6.07	<a href="https://www.mcmaster.com/1227T459/">https://www.mcmaster.com/1227T459/</a>	Acrylic
Sample Holder Top	8531K21	1	\$18.96	\$18.96	<a href="https://www.mcmaster.com/8531K21/">https://www.mcmaster.com/8531K21/</a>	Acrylic
<b>Optical strain mapping</b>						
Dynamically Damped Post	DP14A-POST	1	\$219.67	\$219.67	<a href="https://www.thorlabs.com/newgrouppage9.cfm?objectgroup_id=170&amp;pn=DP14A#170">https://www.thorlabs.com/newgrouppage9.cfm?objectgroup_id=170&amp;pn=DP14A#170</a>	Metal
Lens Holder Assembly	8560K265	1	\$33.98	\$33.98	<a href="https://www.mcmaster.com/acrylic/thickness~1-2/">https://www.mcmaster.com/acrylic/thickness~1-2/</a>	Acrylic
Lens	Tamron M111FM25	1	\$579.00	\$579.00	<a href="https://www.bhphotovideo.com/c/product/1181229-REG/tamron_m111fm50_12mp_50mm_fixed_focal.html">https://www.bhphotovideo.com/c/product/1181229-REG/tamron_m111fm50_12mp_50mm_fixed_focal.html</a>	Component
Camera	BFS-U3-200S6C-C	1	\$729.00	\$729.00	<a href="https://www.flir.com/products/blackfly-s-usb3/?model=BFS-U3-200S6C-C">https://www.flir.com/products/blackfly-s-usb3/?model=BFS-U3-200S6C-C</a>	Electronic component

1

2

## 5. Build Instructions

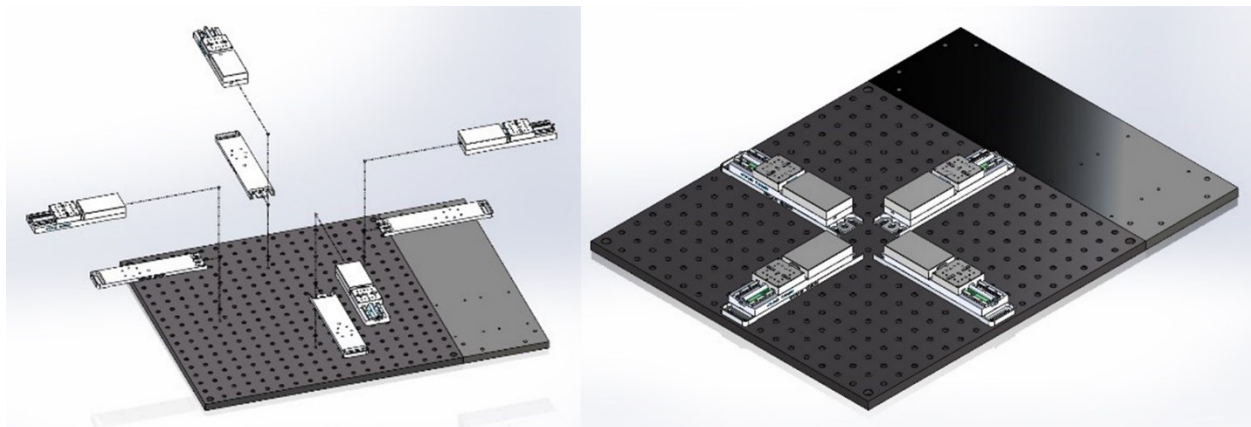
3

### 5.1 Testing Platform

4

The testing platform (**Figure 8**) was built by selecting off-the-shelf parts and components that can easily be assembled and reconfigured if needed. The 18x18" perforated optical breadboard ensures adequate alignment of the four linear actuators in a cruciform configuration. A 18x6" plate was added on the back-end of the system to increase the surface area to 18"x24" and provide enough space for the Servo Motor Drivers. The linear actuators (MTS50-Z8) are attached to the breadboard using Breadboard Mounting Adapters (MTS50A-Z8).

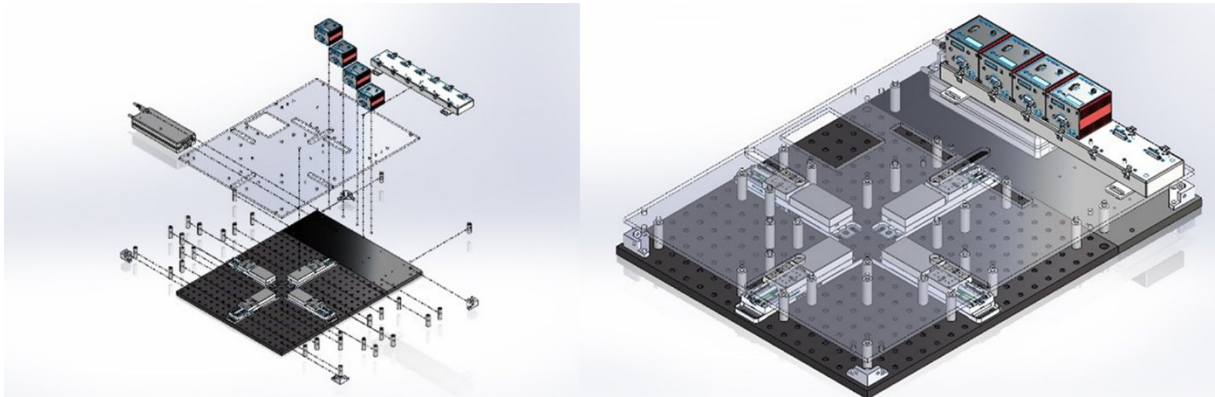
9



10

1           **Figure 8.** Testing platform base. The perforated optical breadboard and back-end plate create a  
2 24" x 24" footprint for building the system. The Breadboard Mounting Adapters (MTS50A-Z8) are  
3 positioned in a cruciform shape on the center of the breadboard, and the linear actuators (MTS50-Z8) are  
4 attached to mounting adapters.

5  
6           The linear actuators are physically isolated from other components by using an acrylic plate  
7 supported by several round standoffs (**Figure 9**). This separation plate also holds in place the USB  
8 Controller Hub where the four DC Servo Motor Drivers are connected. Below the USB Controller Hub the  
9 power supply can be found. The system was designed in SolidWorks, and flat components, such as the  
10 acrylic plate, were manufactured using a CO<sub>2</sub> laser cutter. Other non-flat components, such as the acrylic  
11 corner brackets were in turn fabricated using a Modela Pro II MDX-540 3D milling machine. All  
12 components were attached to the breadboard using ¼-20 female threaded round standoffs and ¼-20  
13 threaded rods.

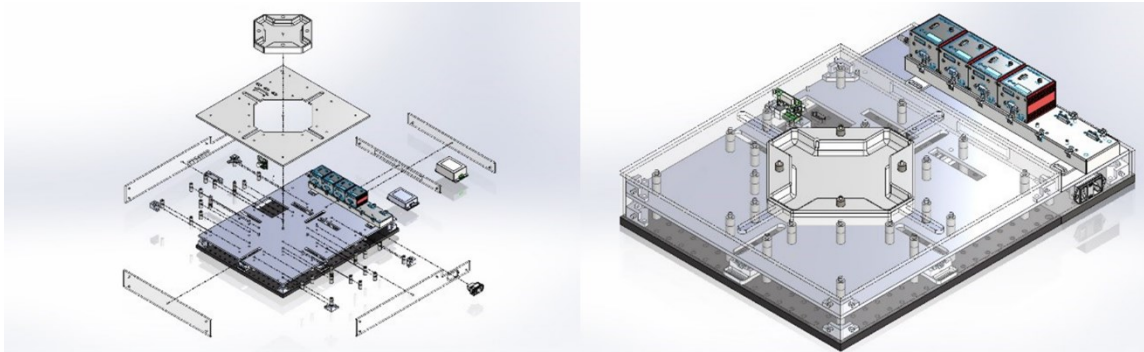


14  
15           **Figure 9.** Testing platform plate. The acrylic plate was attached to the system using ¼-20 female  
16 threaded round standoffs and ¼-20 threaded rods. The USB Controller Hub is placed on top of the acrylic  
17 plate at the back-end of the system. The USB Controller Hub power supply is found under the controller  
18 hub.

## 20           5.2 Specimen Testing Chamber

21           The specimen testing chamber was manufactured using a MDX-540 milling machine. The SolidPart  
22 file from SolidWorks was transformed into STL format and loaded into SRP player to create the milling  
23 paths. The testing chamber was cut from a 12"x12"x2" Polytetrafluoroethylene (PTFE) stock. The top and  
24 lateral side acrylic plates were also manufactured using the laser cutter. These acrylic plates have all  
25 necessary cut through holes to allow the passage of cables, temperature controller, main power switch,  
26 movable parts and the testing chamber (**Figure 10**). The middle and top plates between the linear  
27 actuators and the testing chamber helps isolate the motors from the heating actuator and the fluid in the  
28 testing chamber. The two plates are hold in place by stainless steel threaded studs. The temperature  
29 board is attached to the top plate using a rectangular bracket fabricated in the milling machine. The two

1 power supplies used for the Peltier plate and the W1209 control board are secured on the extension plate  
2 under the USB hub. The heating side of the Peltier thermal actuator is attached using thermal paste to a  
3 4 x 4 x 0.024 in stainless steel plate. The temperature sensor is pressed fit within a sensor hole carved  
4 within the testing chamber.

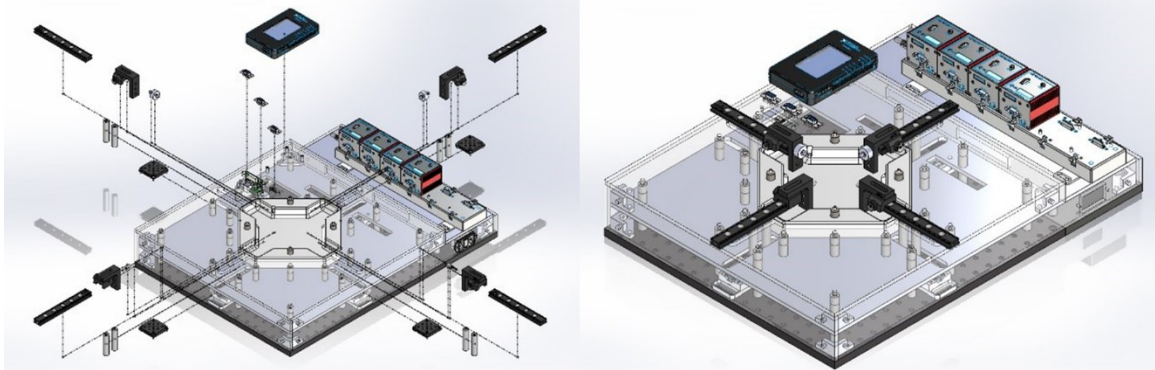


5  
6 **Figure 10.** Specimen testing chamber building. The PTFE testing chamber and top acrylic plate are  
7 hold in place by stainless steel threaded standoffs and threaded rods. The temperature board is attached  
8 to the top plate using a rectangular bracket fabricated in the milling machine. The two power supplies  
9 used for the Peltier plate and the W1209 control board are secured on the back-end plate under the USB  
10 hub. The temperature sensor is pressed fit within a sensor hole carved within the testing chamber.

### 11 12 **5.3 Force Sensing unit**

13 An MTS A1 adapter plate was attached to the movable part of each linear actuator, and two  
14 stainless steel, female threaded round standoffs, are in turn connected to the MTS A1 adapter using  $\frac{1}{4}$ "-  
15 20 threaded rods (**Figure 11**). The dovetail optical rail (RLA0600) is secured on top of the standoffs using  
16  $\frac{1}{4}$ "-20 stainless steel socket head screws. A hinge system was built between the rail carrier (RC1) and a  
17 right angle bracket (AB90C) using two ball bearings (Trade Number R3, for  $\frac{3}{16}$ " shaft diameter) and a  
18 stainless steel dowel pin ( $\frac{3}{16}$ " diameter,  $\frac{7}{16}$ " long). To create this hinge, a  $\frac{1}{2}$ " diameter,  $\frac{3}{16}$ " long cut  
19 was made with the milling machine on the bottom face of the dovetail optical rail and on the counterbore  
20 mounting slot of the right angle bracket. Then a ball bearing was press fit attached into each cut, and the  
21 two movable pieces were connected together placing the dowel pin through the center opening of the  
22 ball bearings. The dovetail optical rail was placed onto the rail, while keeping the right angle bracket inside  
23 the testing chamber. The right angle bracket has three  $\frac{1}{4}$ "-20 tapped holes, and the MSA25 tread adapter  
24 was inserted into one of them to attach the fixed end of a sub-miniature load cell (Honeywell, model 31,  
25 2000g). The cable from the load cell was soldered to a DB-09 male connector so that the load cell can be  
26 easily replaced if needed, and a matching DB-09 female connector was installed on the top acrylic plate  
27 of the system. The DB-09 female terminals are connected inside the system to a load cell signal  
28 conditioner and digitizing circuit (HX711 Sensor). Three DB-09 female connectors are attached to the top  
29 acrylic plate and wired to the inputs of three HX711 load sensing boards. Each HX711 board has a full  
30 Wheatstone bridge configuration to sense changes in the load cell, followed by the HX711 microchip, a  
31 precision 24-bit analog to digital converter with low-noise programmable gain amplifiers. The HX711 uses  
32 a two-wire interface (Clock and Data) for synchronization and data transfer (80SPS) with a GPIO. The  
33 digital outputs of the HX711 board are connected to ribbon cable connectors located on the left side wall

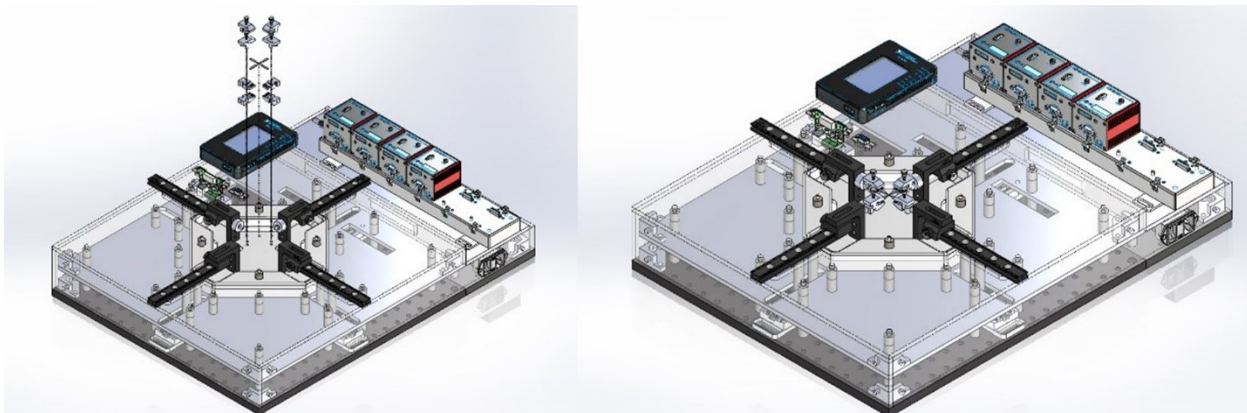
1 of the system. A Ribbon cable then links the digital outputs of the system to the myRIO-1900 board. This  
2 portable reconfigurable I/O device allows for real time acquisition of load cell data from the HX711 board  
3 into a computer for recording and visualization of data. The myRIO-1900 board is attached to the cover  
4 plate of the system next to the DB-09 female connectors.



5  
6 **Figure 11.** Force Sensing Unit. An MSA1 adapter plate is attached to the movable part of each  
7 linear actuator and supports two round standoffs that link the actuators to the dovetail optical rail  
8 (RLA0600). The adjustable rail carrier has a low friction hinge connecting to the right angle bracket  
9 (AB90C). A MSA25 tread adapter was inserted into the right angle bracket to attach a sub-miniature load  
10 cell (Honeywell, model 31). The load cell is connected to a signal conditioner and digitizing circuit (HX711  
11 Sensor). The digital outputs of the HX711 board are connected to a portable reconfigurable I/O device  
12 (myRIO-1900 board).

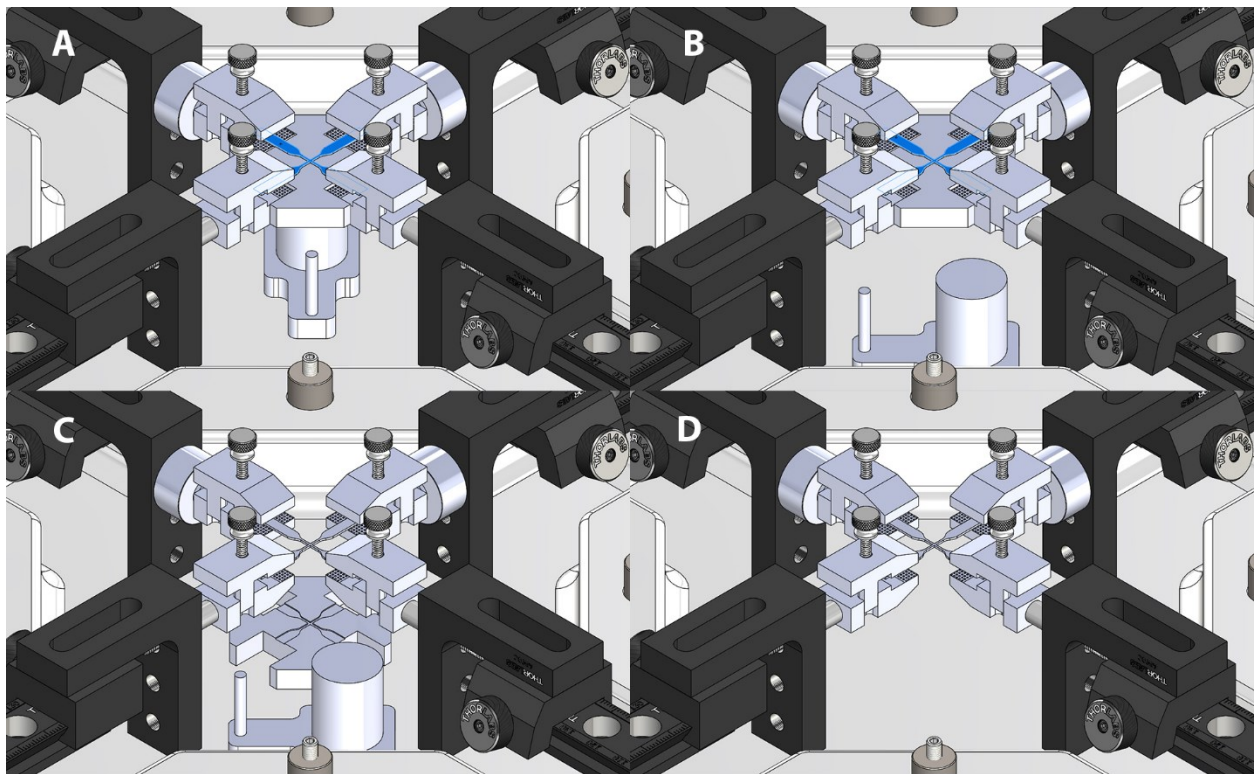
#### 13 5.4 Tissue Gripping mechanism

14 The small custom made clamps were first prototyped in ABS plastic using a 3D printer, followed  
15 by manufacturing using the 3D milling machine using acrylic and aluminum. Both clamp jaws have small  
16 pyramids to increase the friction between the clamp and the sample, and thus reduce the possibility of  
17 slippage. Different designs were tested until obtaining a clamp with the smallest footprint and volume, so  
18 to minimize the weight that is attached to the end of the load cell. The jaws of the final clamp design  
19 remain always well aligned by the vertical slot and pin built in within the clamp design. The thumbscrew  
20 secures the two jaws of the clamp, while maintaining their surfaces well aligned and parallel to provide a  
21 uniform holding force on the sample (**Figure 12**).



1           **Figure 12.** Tissue gripping mechanism. Small custom-made clamps have two opposing jaws with  
2 small pyramids to reduce the possibility of sample slippage. The jaws of the clamp design are self-aligned  
3 by the vertical slot and pin built in within the clamp design. A uniform holding force is achieved using a  
4 thumbscrew that secures the two jaws of the clamp.

5           A sample holder was designed to help mounting the sample into the system at the center of the  
6 2 axes (**Figure 13**). The sample holder comprises two components, the top holder has a groove with the  
7 shape of the biaxial sample, and can hold either uniaxial or biaxial samples. The top holder also has four  
8 extruded cuts to hold the bottom part of the clamp in place, aligned with its dovetail optical rail. The  
9 bottom holder component has a cylinder, a plate and a handle. Initially, the bottom holder is placed at  
10 the center of the testing chamber, the top holder component is placed on top of its bottom counterpart  
11 and aligned with the lower part of the clamp. The sample is then placed at the center of the sample holder  
12 and the top portion of the clamps are set in place and secured with the thumbscrews. Once the sample is  
13 secured, the bottom holder component is removed by sliding it carefully away from the center of the  
14 system, and the top holder portion is moved down and removed from the testing chamber. The use of  
15 this sample holder allow us to set the sample at the center of the system, well aligned with the actuation  
16 axes.



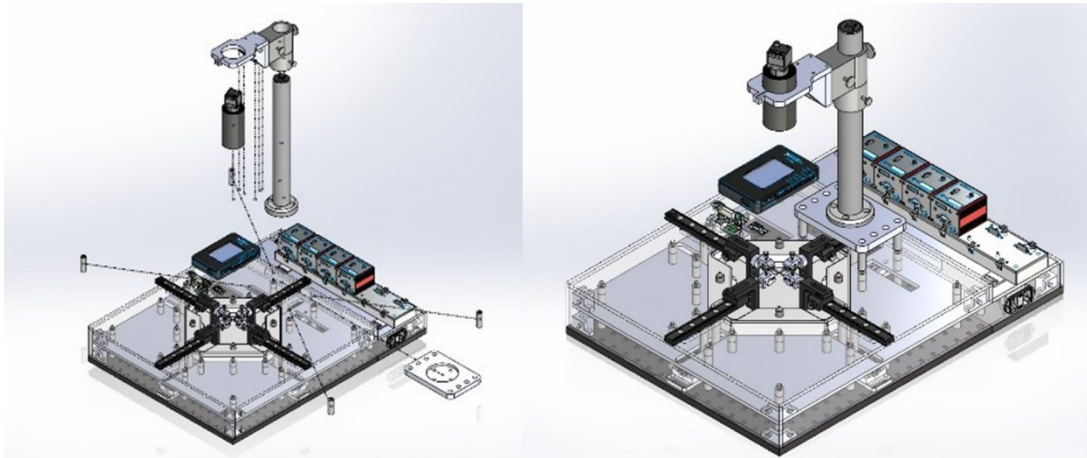
17  
18           **Figure 13.** Tissue holding and alignment system. The sample holder has a top holder and a  
19 removable bottom holder. (A) The bottom holder component is placed at the center of the testing  
20 chamber, the top holder component is placed on top of its bottom counterpart and aligned with the lower  
21 part of the clamp. The sample is then placed at the center of the sample holder and the top portion of the  
22 clamps are set in place and secured with the thumbscrews. (B) Once the sample is secured, the bottom

1 holder component is removed by sliding it carefully away from the center of the system, and (C) the top  
2 holder portion is moved down and (D) removed from the testing chamber. The use of this sample holder  
3 allow us to set the sample at the center of the system, well aligned with the actuation axes.

4

### 5 5.5 Digital Image Correlation System

6 Four standoff pints were attached on top of the top acrylic plate to support a custom acrylic  
7 camera holder plate. A round post is secured with four screws into the camera holder plate and a lens  
8 bracket was attached to the camera post (**Figure 14**). The custom lens holder was manufactured in the 3D  
9 milling machine and has an opening through which the Machine Vision lens is inserted and secured  
10 using a set screw. The digital camera is attached to the back of the lens using a C-mount adapter and connected  
11 to the computer using a USB3 with power cable. The dimensions of the lens holder were chosen so that  
12 the center of the camera field of view coincides with the center of the system where the sample will be  
13 stretched. The positioning of the holder can be adjusted vertically to modify the ROI in the image, or by  
14 modifying the focal plane of the lens.



15

16 **Figure 14.** Digital Image correlation system. Four standoff pints support a custom acrylic camera  
17 holder plate, a round post, camera holder plate and a lens bracket. The Machine Vision lens is inserted in  
18 the camera holder, the digital camera is attached to the back of the lens using a C-mount adapter and  
19 connected to the computer using a USB3 with power cable. The ROI in the image and focal plane of the  
20 lens can be adjusted by either modifying the position of the camera holder or by adjusting the lens focal  
21 distance.

## 22 6. Operation Instructions.

### 23 *Initialization of the System*

24 Turning on the main switch of the system provides power to the USB hub, DC Servo controllers,  
25 and the NI MyRIO system. The USB hub and DC servo controllers run an initialization routine to check the  
26 communication with the PC, and then stay in standby. The high resolution camera is turned on once its  
27 USB cable is connected to the PC. There is no on/off switch for the camera, thus, the USB cable needs to  
28 be unplugged to turn off the camera. The communication between these devices and the PC can be set  
29 and/or troubleshot using NIMax software in case of any communication problem. The next step is to

1 run the LabView software interface, and start the Labview project “BiMaTS.lvproj”. This project comprises  
2 a virtual interface file that resides in the local PC, and a link to a “MyRIO-1900” target device. In turn, the  
3 MyRIO-1900 device has a real time virtual interface file to acquire data from the load cells, and a VI  
4 recorded within the FPGA of the target device. It is only required to run the VI in the local PC “BiMATS.vi”  
5 to initialize and get started the VIs in the PC, target device and FPGA. The Graphic User Interface will  
6 appear on screen, and it is necessary to click on “Run” or select the menu “Operate”, followed by “Run”,  
7 or use the hotkeys “CTR+R”. The DC Servo driver will follow a homing sequence and the load cell(s) will  
8 start acquiring data that is displayed in the force window. If the test is performed under immersion, the  
9 heating system can be switched on to warm up the fluid in the chamber for about 30 minutes, until the  
10 desired temperature is achieved. This warm-up period will also help the load cells to reach a stable  
11 operating temperature.

### 12 *Mounting Samples*

13 Silicone samples are prepared using a mold and curing the material in a laboratory oven. This  
14 approach provide samples with consistent shape and size, according to ASTM Standard D412 “Tension  
15 Testing for Rubber and Elastomers”. The sample surface is sprayed with acrylic ink droplets for speckle  
16 recognition using DIC for strain measurements. DIC is used to obtain more accurate data as it enables  
17 measuring the strain directly at the sample’s surface. Depending on the size of the samples being tested,  
18 the distance between grips can be adjusted to maintain the region of interest at the center of the camera  
19 field of view. The distance between grips is easily adjusted using the dovetail rail carriers, without moving  
20 the linear actuator from the zero position. The top section of the clamp is removed and the sample is  
21 placed on top of the bottom clamp jaw, and fastened by the top clamp. The small pyramids on the clamp  
22 jaw help providing increased friction with the sample to avoid the possibility of slippage. When setting  
23 the samples into the grips, ensure to not apply excessive force at the grip-sample interface when manually  
24 tightening the screw, to avoid damaging the sample. When working with biaxial samples, fix the sample  
25 arms into the grips opposite to each other first, then adjacent grips. The camera lighting can be adjusted  
26 at this stage to obtain the best images possible at the center of the sample’s region of interest.

27

### 28 *Operation of Software Interface for mechanical test*

29 When the LabView project file is started, the project file initializes the software, creates the  
30 variables, runs the data acquisition code inside the myRIO interface, the initialization of the camera and  
31 the connection between the software and each of the servo driver hardware by reading and comparing  
32 the serial number defined for each axis and the serial number embedded in the hardware. The next  
33 automated step is to run an initialization routine where the actuators read the desired velocity and  
34 acceleration entered by the user, and move the actuator a few millimeters forward, followed by a home  
35 cycle, where all the actuators are moved backwards to the zero position. The camera field of view is  
36 displayed in the Image Preview window, but they are not recorded in the computer, so that the user can  
37 adjust the field of view or the focus of the lens. The system is ready for operation, and once the user has  
38 placed the sample in the system, it is recommended to perform a preconditioning of the sample, where  
39 the sample is stretched cyclically within a displacement range that would not lead to rupture (e.g. n=10  
40 cycles, 50% stretch), and will reduce hysteresis and the possibility of sample slippage. The user can select  
41 the number of cycles, file name and file path for data and images. The preconditioning can be performed

1 for uniaxial or biaxial tests. After preconditioning of the sample, the user may chose performing a uniaxial  
2 or a biaxial test by selecting the corresponding tab in the GUI, next to the right of the preconditioning tab.  
3 The user can select the file name and path for recording the force, displacement, time and images being  
4 acquired during the test. The user may also choose to run a homing cycle, and return the actuators to the  
5 zero position, at the end of a test. Preconditioning, uniaxial and biaxial tabs have an Image Recording  
6 window that shows the images that are being stored in the PC hard drive during the test. Once  
7 preconditioning is completed, the user will enter the target displacement for the horizontal and/or the  
8 vertical direction. The presence of two distinct tabs for the target displacements in the horizontal and  
9 vertical directions allows to perform two types of biaxial loading: (1) the target displacement, velocity and  
10 acceleration are imposed in the two tensile directions; (2) the target displacement, velocity and  
11 acceleration are imposed in one tensile direction while the position of the sample in the other direction  
12 is maintained constant. The user has the possibility of easily defining any other desired motion sequence.  
13 Tare the load cells (set to zero) before starting the test, to ensure zero offset of the force readings. Force  
14 and displacement are acquired simultaneously at a high rate using Real-time VIs at the MyRIO-1900  
15 system, temporally stored in the MyRIO-1900, and then transferred to the PC at a lower rate. Images  
16 acquisition and recording were automatically started by the initiation of the test, and automatically  
17 stopped when the target range of motion is achieved. Data is recorded using the TDMS format (Labview,  
18 National Instruments), and images are stored as JPEG. Force, displacement, and time can be easily  
19 exported into Matlab for analysis, and the sequence of images taken during the test are also exported  
20 into GOM Correlate Software to calculate engineering stress and strain, and then determine true stress  
21 and strain. These experimental data can be used in general for determining the material properties of  
22 tissues and soft materials. The non-linear behavior of soft materials can also be used to curve fit  
23 constitutive models and characterize their parameters. In particular, the ultimate stress, strength and  
24 strain at failure can be determined.

## 25 **7. Validation and Performance Characterization**

### 26 *Actuation System: Displacement and Actuators Velocity*

27 The linear motion performance of the system was characterized using a series of tests. First, to  
28 validate each linear stage motion accuracy, we compared different target displacement values introduced  
29 in the LabView interface versus measurements of displacement recorded using a digital caliper. We  
30 performed five tests with different target displacements in the x- and y- directions, and measured the  
31 initial separation distance of the translation stages with the caliper. After each target displacement was  
32 reached, we measured the total distance and repeated the experiment after bringing back the stage to  
33 the zero position ( $n = 10$  independent measurements at each target position) with the electronic caliper.  
34 In both x- and y-directions, our analysis showed a high level of linearity and coefficients of determination  
35 ( $R^2 = 0.9997$  and  $0.9998$ , respectively), proving that the motorized translation stages can reach the target  
36 displacement with high accuracy.

37 The Thorlabs servo motor controller and LabVIEW software are the hardware and software  
38 components that control the velocity of the motorized translation stage. A test was carried out to evaluate  
39 the system's ability to accurately achieve the desired actuator velocity inputted in the LabView interface.  
40 This measurement was repeated ( $n = 10$  independent measurements at each target actuator velocity) for  
41 different clamps velocities: 0.02, 0.1, 0.2, 1.0, 2.0, 3.0, 4.0, and 4.8 mm/s, in the x- and y-direction. After  
42 each set of tests, the mean actuator velocity was compared to its respective target velocity recorded using

1 the digital position sensor of the linear stage. Our analysis shows that the translation stages are capable  
 2 of maintaining the actuators velocity consistently in both directions, with 99.0 – 100% accuracy, and mean  
 3 coefficients of determination ranging  $R^2 = 0.9992-1.0$ . The experiments reported below were performed  
 4 using an actuator velocity of 1.0 mm/s, for which we found an accuracy of 100% due to the fast feedback  
 5 system of the linear stage.  
 6

7 *Actuation System: Load Cell*

8 Measurement of the reaction force produced by a testing sample is achieved using sensitive  
 9 miniature load cells (Model 31, Honeywell). We calibrated the load cell used in both axes of the system as  
 10 follow: we used an L-bracket to position two standoffs and a dovetail optical rail vertically. The rail carrier  
 11 is attached to the optical rail and the load cell is secured vertically at the end of the rail carrier. Weights  
 12 (20g - 500g) were hung from the load cell to acquire a calibration curve between the output voltage of  
 13 the load cell and the calibration weights. The slope of the calibration curve or scale factor was determined  
 14 using a straight line curve fitting to the data. This test was repeated ten times, and the mean measured  
 15 weight was compared to the actual (nominal) weight. **Table 4** shows the mean measurement weight, the  
 16 accuracy of the measurement (94.0-99.9%), and the coefficient of variance between each of the tests for  
 17 each weight value (CV = 0-0.02).

18 **Table 4:** Accuracy and Coefficient of Variation of weight measurements acquired with the x- and  
 19 y-direction load cells.

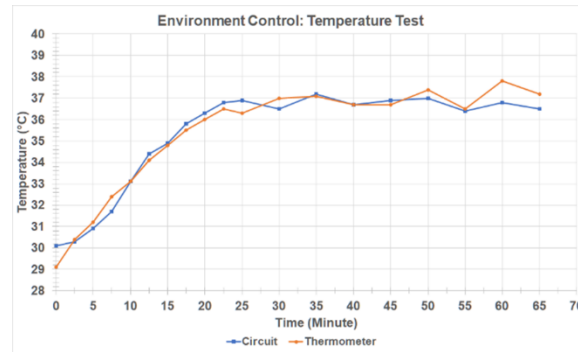
X-direction Load Cell			
Weight (g)	Measured Weight Mean ± SD (g)	Accuracy of Measurement (%)	Coefficient of Variation
0	0	-	0
20	19.85 ± 0.43	99.3%	.02
50	50.10 ± 0.44	99.8%	0.009
100	100.01 ± 0.12	99.9%	0.001
200	200.13 ± 0.05	99.9%	0.0002
500	499.77 ± 0.54	99.5%	0.001
Y-direction Load Cell			
Weight (g)	Measured Weight Mean ± SD (g)	Accuracy of Measurement (%)	Coefficient of Variation
0	0	-	0
20	18.80 ± 0.27	94.0%	0.01
50	48.38 ± 0.24	96.8%	0.005
100	98.37 ± 0.26	98.4%	0.003
200	199.57 ± 0.46	99.8%	0.0023
500	501.35 ± 1.14	99.7%	0.0023

20

21 *Environment Control: Temperature*

22 To obtain testing conditions similar to the physiological environment, the specimen chamber  
 23 needs to maintain a constant temperature of the medium during the experiment. The validation test was  
 24 designed to evaluate how long it would take for the water in the chamber to reach a temperature range  
 25 of  $37.0 \pm 1.0^\circ\text{C}$  and sustain it for a long period of time. The readings of the W1209 circuit were compared  
 26 to a standard digital thermometer for accuracy. **Figure 15** shows that the initial temperature of the water

1 in the specimen chamber as per the thermometer readings was 29.1°C, while the W1209 circuit read  
2 30.1°C. At the 25-minute mark, the temperature circuit reached 37.0°C. After this point, the temperature  
3 was monitored for 40 minutes and the circuit was able to maintain a temperature range of 37.0 ± 1.0°C.  
4 The thermometer's lowest temperature reading was 36.5°C and the highest temperature reading was  
5 37.8°C. It was surmised that the temperature circuit is capable of providing a warm environment for future  
6 studies.



7  
8 **Figure 15:** Dynamics of temperature. The temperature control system warms up the fluid in the testing  
9 chamber. The graph presents a comparison of temperature recorded from the temperature controller  
10 and the temperature measured with a thermocouple-based thermometer.

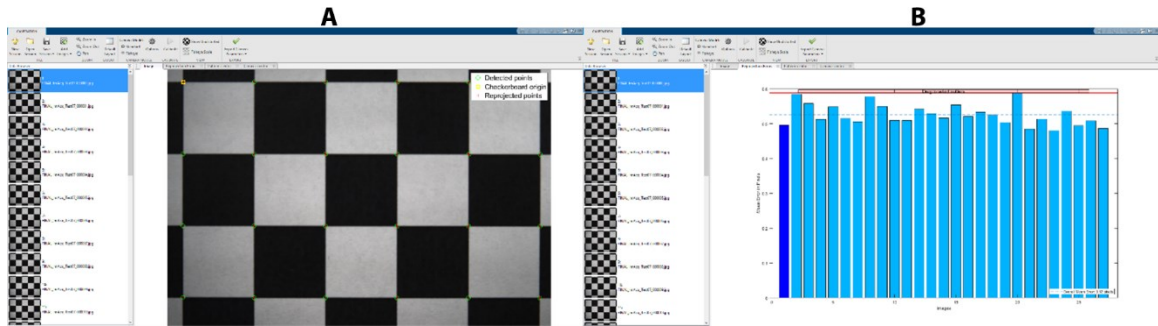
### 11 *Gripping Mechanism: Slippage*

12 The ability of the grips to prevent slippage of the sample was also evaluated. If the sample slips  
13 during the tensile test, the overall stress will decrease, either causing the recorded data to be skewed or  
14 prevent rupture. A test was designed where one sample was stretched in the x- and y-direction. A marked  
15 region (3.8 mm) of the sample was placed in the gripping mechanism and the samples were stretched 10  
16 times for 10 mm. Each time, a caliper was used to measure any possible grip slippage as well as images  
17 were taken for digital measurement. After performing the evaluation test in the x- and y- directions 10  
18 times, there was no noticeable or measurable slippage of the sample.

### 19 *Strain Measurement: Image Analysis & Strain Mapping*

20 The digital camera was calibrated using the Computer Vision Toolbox and the cameraCalibrator  
21 app in Matlab (V. 2021b, Mathworks). A 10x10 checkerboard pattern image was created comprising black  
22 and white 10mm x 10mm squares with 1200dpi resolution. The checkerboard pattern was printed using  
23 a high resolution printer (ColorLaserJet Pro MFP M476dw, Hewlett Packard) and placed in a flat surface  
24 at the focal distance of the Tamron M111FM25 lens. Ten images were acquired by the system and loaded  
25 into the cameraCalibrator app in Matlab. The camera field of view (5472 x 3648 pixels) comprises at least  
26 4 by 6 squares of the checkerboard pattern. The cameraCalibrator app detects the checkerboard corners  
27 in the images and generates the coordinate system in millimeters (**Figure 16A**). The camera parameters  
28 (accuracy, skew and lens distortion errors) were calculated for each image based on the position of the  
29 checkerboard corners within the coordinate system and estimate the reprojection errors in pixels. The  
30 bar graph (**Figure 16B**) indicates that the accuracy of the calibration is 0.53 pixels, where each bar  
31 represents the mean reprojection error for the corresponding calibration image. The reprojection errors

1 are the distances between the corner points detected in the image, and the corresponding ideal points  
2 projected into the image. The estimated skew error is 3.63 pixels, the radial distortion coefficients are  
3  $k_1=0.036$  and  $k_2=62.847$ , and the tangential distortion coefficients of the lens are  $k_1=0.003$  and  $k_2=0.002$ ,  
4 where  $x_{distorted} = x(1 + k_1r^2 + k_2r^4)$ ,  $y_{distorted} = y(1 + k_1r^2 + k_2r^4)$ ,  $x$  and  $y$  are the undistorted  
5 pixel locations and  $r^2 = x^2 + y^2$ . The measured camera parameters obtained by the cameraCalibrator  
6 app are used for correcting the measured distortion and produce distortion-free images.  
7



12 **Figure 16:** Camera Calibration and accuracy measurement. (A) The original checkerboard image (1.0 cm x  
13 1.0 cm) with the corners detected (green circles) and the reprojected points (red crosshair markers). (B)  
14 Histogram of mean error in pixels for each analyzed image, showing an overall mean error of 0.53 pixels.  
15

16 The quality of the DIC analysis largely relies on the speckles pattern of the sample being analyzed.  
17 To obtain accurate and reliable data, we followed the recommendations for good DIC testing [17]. First,  
18 the paint used for the pattern should be of high contrast against the samples' color. Since the material  
19 tested in this study is transparent, we used a water-based black ink. Then, the speckles size should be in  
20 the range of 3-5 pixels and the pattern density between 20-50% of the sample's area. We used a  
21 professional airbrushing paint system (VIVOHOME, California, USA) to ensure a constant speckle size and  
22 a uniform pattern. The spraying technique was optimized using the pattern quality assessment available  
23 in GOM Correlate.  
24

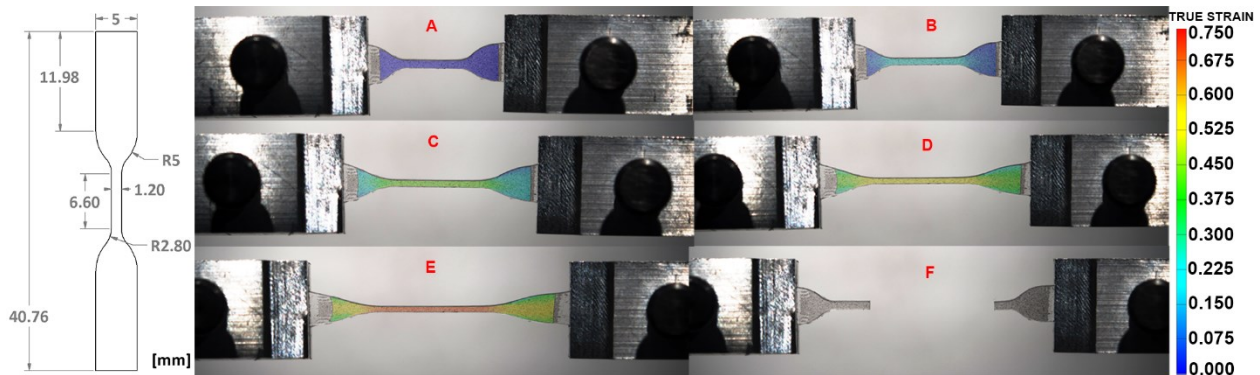
25 Once images are imported into GOM, the user selects the size of squared facets and their  
26 respective overlapping area to be used for further calculations. To ensure accurate results, the facet  
27 should contain at least three pattern points so that one subset can be distinguished from all other subsets  
28 in the ROI. In this study, we used a facet size of 17x17 pixels and a point distance of 15 pixels, which gave  
29 the best outcome in terms of pattern quality.  
30

### 31 *Uniaxial and biaxial Tensile tests*

32 To evaluate our tensile test protocol, we tested ten uniaxial samples in the axial direction, and ten  
33 biaxial samples in both x- and y-directions until rupture. The polymer mixture that was used for preparing  
34 the testing samples is Polydimethylsiloxane (PDMS, or Sylgard 184, Dow Corning). Sylgard 184 [18-21] is  
35 a widely used elastomer in the scientific community due to its biocompatibility, optical transparency,  
36 flexibility and mechanical properties. Given its ability to change elasticity depending on the base to curing  
37 agent ratio, Sylgard184 has been often considered as a laboratory model material for different soft tissues  
38 [22-24]. Samples were prepared with a base to curing agent ratio of 10:1, cured at a temperature of 100°C

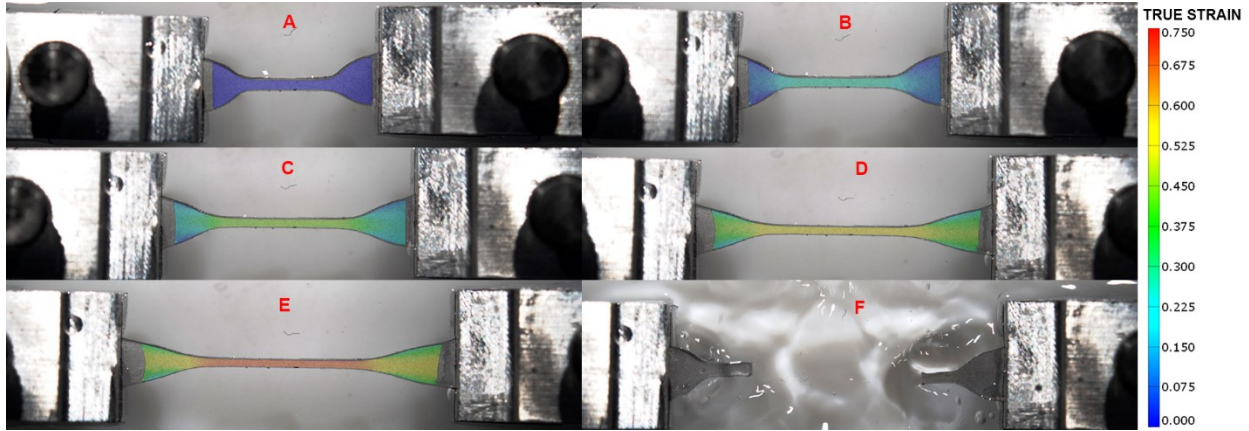
1 and then sprayed to create the speckle pattern needed for DIC. For uniaxial tests, dumbbell-shape samples  
2 was scaled-down to 20% of original ASTM D412 standard sample size for tensile testing of rubbers and  
3 elastomers (**Figure 17**), with a thickness of 0.6mm. For biaxial tests, cruciform samples were derived from  
4 the uniaxial geometry, maintaining the same dimensions (**Figure 20A**)

5 The experimental procedure consisted of applying 10-cycles preconditioning stretch at 10% strain,  
6 followed by one-single pull to rupture. **Figure 17** demonstrates the progression of the strain in the ROI of  
7 one sample from the undeformed state until failure. **Figure 17A** shows the sample in the unloaded  
8 configuration. As the translation stages move to the target displacement, the program is able to map the  
9 strain profile of the material. In **Figure 17E**, the gauge region has reached the ultimate strain of polymer  
10 mixture and in **Figure 17F**, the sample has ruptured, and the strain map ends.



11 **Figure 17: (Left)** Technical drawing of the uniaxial sample, from the standard ASTM D412-Type C. **(Right)**  
12 **Strain map of a uniaxial sample of Sylgard184 (n=10) calculated in GOM Correlate in empty bath. (A)**  
13 **Sample is in its underformed state. (B-E) Sample is progressively stretched and the increase in strain is**  
14 **mapped on its surface. (F) Sample has ruptured in the gauge region, where strain is the highest.**  
15

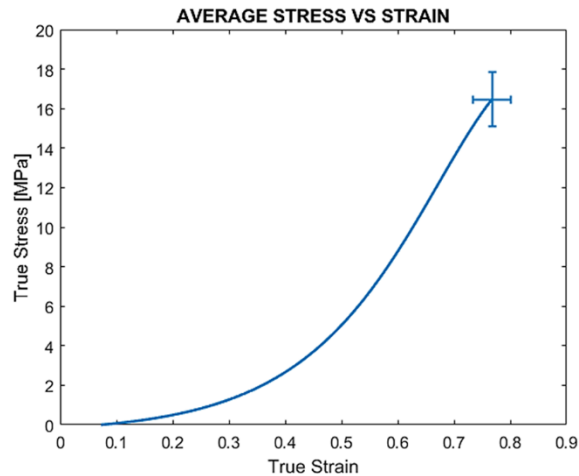
16  
17 When studying soft tissues, the sample should ideally be maintained in a bath of physiological  
18 solution. To validate the DIC analysis when testing samples in solution, we also performed experiments  
19 where our bath was filled with water until wetting the sample and keeping it humid throughout the test.  
20 In this case, we sprayed the samples using black acrylic paint, so that the pattern wasn't washed away by  
21 the fluid. The strain mapping until rupture is reported in **Figure 18**. The software was able to calculate  
22 the strain profile for all stretch levels and the ultimate strain reported was the same as for samples tested  
23 on the bath without water. These results validate the strain mapping protocol when using our device  
24 whether the samples can be kept dry or need to be tested in physiological solution.  
25



1  
2 **Figure 18:** Strain map of a uniaxial sample of Sylgard184 calculated in GOM Correlate in bath filled with  
3 water. (A) Sample is in its undeformed state. (B-E) Sample is progressively stretched and the increase in  
4 strain is mapped on its surface. (F) Sample has ruptured in the gauge region, where strain is the highest,  
5 causing fluid perturbation on its surrounding.

6

7 The true stress values were calculated by deriving the reduction in cross-sectional area from the  
8 change in width in the gauge region throughout the test, assuming the material as isotropic. The individual  
9 and average true stress and strain curves were obtained combining the data from the tensile system and  
10 the DIC analysis in a custom-made MATLAB script. The average response of the material under uniaxial  
11 tension is reported in **Figure 19**, which shows the typical hyperelasticity of Sylgard 184. Our results agree  
12 with data previously reported in the literature for Sylgard 184 [25-27], demonstrating the reliability of our  
13 system.

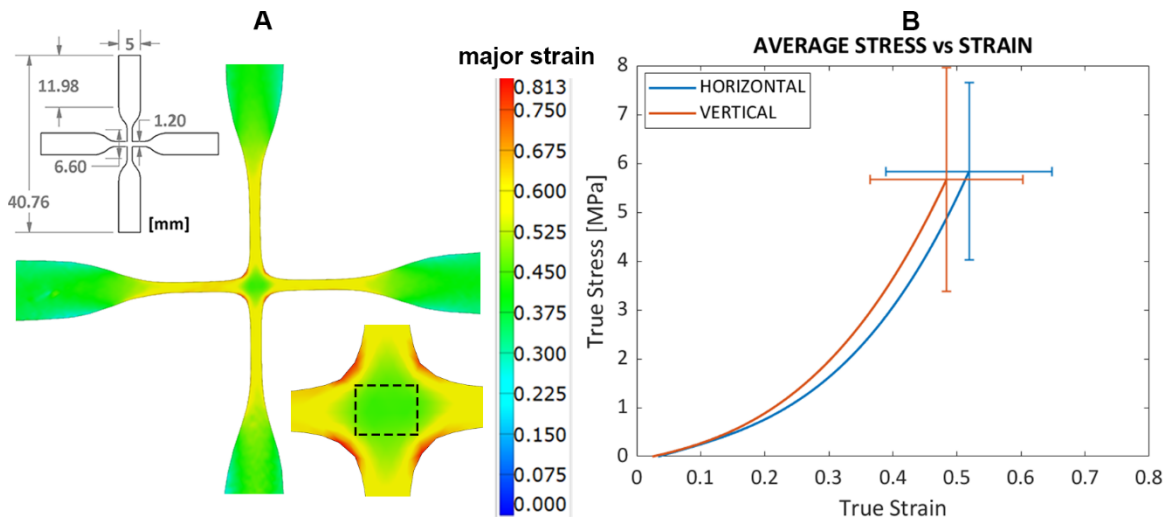


14

15 **Figure 19:** Average true stress-strain curve for Sylgard 184 (n=10), calculated with DIC analysis. Error bars  
16 represent  $\pm$ SD of ultimate stress and strain.

17 The results for biaxial tests are reported in **Figure 20**. For this case, since the material exhibits the  
18 highest engineering stresses measured by DIC at the central corners (**Figure 20A**) and always failed at that  
19 location, it was not possible to derive the change in cross-section area in this region. Thus, to calculate

1 the true stresses, we first derived the engineering strain from the true strain values obtained in GOM and  
 2 then computed the Cauchy stresses for each sample in the two directions. The strain data were extracted  
 3 from the test region where the strain field is uniform. The average true stress and strain curves in the  
 4 longitudinal (horizontal) and vertical direction are reported in **Figure 20B** and show no significant  
 5 difference between the two directions of loading. Our results show the ability of our system to perform  
 6 and record accurate data for a biaxial tensile test. The material exhibits a mechanical response that is very  
 7 close in the horizontal and vertical direction, confirming its isotropic nature.



8  
 9 **Figure 20:** Testing of biaxial sample of Sylgard184 (n=10). (A) Technical drawing of the cruciform sample;  
 10 Two-dimensional mapping of the true major strain of one sample from GOM, with a closer view of the  
 11 test region, showing the uniform strain field in the central area. (B) Average true stress-strain curves for  
 12 the two tensile directions.

13

14

## 15 8. Acknowledgements

16 Financial support for the conduct of the research was provided by NSF grants CMMI-1662970,  
 17 MRI-2018485, PSC-CUNY 64696-00 52, and CUNY IRG program. The funding source(s) had no involvement  
 18 in the study design; in the collection, analysis and interpretation of data; in the writing of the report; and  
 19 in the decision to submit the article for publication.

20

## 21 9. Declaration of interest: none

22

## 23 10. References

24

- 25 1. Azadani, A.N., et al., Comparison of mechanical properties of human ascending aorta and aortic  
 26 sinuses. *Ann Thorac Surg*, 2012. 93(1): p. 87-94.
- 27 2. Benedik, J., et al., Comparison of ascending aortic cohesion between patients with bicuspid  
 28 aortic valve stenosis and regurgitation. *Eur J Cardiothorac Surg*, 2014. 46(6): p. e89-93.

- 1 3. Fehervary, H., et al., Planar biaxial testing of soft biological tissue using rakes: A critical analysis  
2 of protocol and fitting process. *J Mech Behav Biomed Mater*, 2016. 61: p. 135-151.
- 3 4. Fehervary, H., et al., How important is sample alignment in planar biaxial testing of anisotropic  
4 soft biological tissues? A finite element study. *J Mech Behav Biomed Mater*, 2018. 88: p. 201-  
5 216.
- 6 5. Fata, B., et al., Regional structural and biomechanical alterations of the ovine main pulmonary  
7 artery during postnatal growth. *J Biomech Eng*, 2013. 135(2): p. 021022.
- 8 6. Imsirovic, J., et al., Design of a Novel Equi-Biaxial Stretcher for Live Cellular and Subcellular  
9 Imaging. *PLoS One*, 2015. 10(10): p. e0140283.
- 10 7. Li, L., et al., A miniaturized biaxial tensile apparatus based on torsional loading design. *Rev Sci*  
11 *Instrum*, 2019. 90(4): p. 045103.
- 12 8. Potter, S., et al., A Novel Small-Specimen Planar Biaxial Testing System With Full In-Plane  
13 Deformation Control. *J Biomech Eng*, 2018. 140(5).
- 14 9. Faturechi, R., A. Hashemi, and N. Abolfathi, A tensile machine with a novel optical load cell for  
15 soft biological tissues application. *J Med Eng Technol*, 2014. 38(8): p. 411-5.
- 16 10. Sang, C., Maiti, S., Fortunato, R. N., Kofler, J., Robertson, A. M., *A Uniaxial Testing Approach for*  
17 *Consistent Failure in Vascular Tissues*. *J Biomech Eng*, 2018. 140(6).
- 18 11. Jiang, M., et al., *A versatile biaxial testing platform for soft tissues*. *J Mech Behav Biomed Mater*,  
19 2021. 114: p. 104144.
- 20 12. King, J.D., S.L. York, and M.M. Saunders, *Design, fabrication and characterization of a pure*  
21 *uniaxial microloading system for biologic testing*. *Med Eng Phys*, 2016. 38(4): p. 411-6.
- 22 13. Shiwarski, D.J., et al., *3D printed biaxial stretcher compatible with live fluorescence microscopy*.  
23 *HardwareX*, 2020. 7.
- 24 14. Jiang, M., et al., *Clamping soft biologic tissues for uniaxial tensile testing: A brief survey of*  
25 *current methods and development of a novel clamping mechanism*. *J Mech Behav Biomed*  
26 *Mater*, 2020. 103: p. 103503.
- 27 15. Bell, B.J., E. Nauman, and S.L. Voytik-Harbin, *Multiscale strain analysis of tissue equivalents using*  
28 *a custom-designed biaxial testing device*. *Biophys J*, 2012. 102(6): p. 1303-12.
- 29 16. Deplano, V., et al., *Biaxial tensile tests of the porcine ascending aorta*. *J Biomech*, 2016. 49(10):  
30 p. 2031-2037.
- 31 17. Jones, E.M.C., et al., *A Good Practices Guide for Digital Image Correlation*, in *International Digital*  
32 *Image Correlation Society*. 2018. p. 94.
- 33 18. Johnston, I.D., et al., *Mechanical characterization of bulk Sylgard 184 for microfluidics and*  
34 *microengineering*. *Journal of Micromechanics and Microengineering*, 2014. 24(3): p. 1-7.
- 35 19. Mata, A., A.J. Fleischman, and S. Roy, *Characterization of polydimethylsiloxane (PDMS)*  
36 *properties for biomedical micro/nanosystems*. *Biomed Microdevices*, 2005. 7(4): p. 281-93.
- 37 20. Wu, C.L., et al., *Static and dynamic mechanical properties of polydimethylsiloxane/carbon*  
38 *nanotube nanocomposites*. *Thin Solid Films*, 2009. 517(17): p. 4895-4901.
- 39 21. Schneider, F., et al., *Mechanical properties of silicones for MEMS*. *J. Micromechanics*  
40 *Microengineering*, 2008. 18(6): p. 1-9.
- 41 22. Ramesh, R., et al., *Comparison of radial expansion of stents within mock vessels molded with a*  
42 *target bent radius versus straight mock vessels bent to a target radius*. *Biomed Sci Instrum*,  
43 2008. 44: p. 189-94.
- 44 23. Hecker, L., et al., *Development of a three-dimensional physiological model of the internal anal*  
45 *sphincter bioengineered in vitro from isolated smooth muscle cells*. *Am J Physiol Gastrointest*  
46 *Liver Physiol*, 2005. 289(2): p. G188-96.

- 1 24. Colombo, A., et al., *A method to develop mock arteries suitable for cell seeding and in-vitro cell*  
2 *culture experiments*. *J Mech Behav Biomed Mater*, 2010. **3**(6): p. 470-7.
- 3 25. Liu, M. and Q. Chen, *Characterization study of bonded and unbonded polydimethylsiloxane*  
4 *aimed for bio-micro-electromechanical systems-related applications*. *Journal of*  
5 *Micro/Nanolithography, MEMS, and MOEMS*, 2007. **6**(2).
- 6 26. Liu, M., J. Sun, and Q. Chen, *Influences of heating temperature on mechanical properties of*  
7 *polydimethylsiloxane*. *Sensors and Actuators, A: Physical*, 2009. **151**(1): p. 42-45.
- 8 27. Liu, M., et al., *Thickness-dependent mechanical properties of polydimethylsiloxane membranes*.  
9 *Journal of Micromechanics and Microengineering*, 2009. **19**(3).